Study of thin film poly-crystalline CdTe solar cells presenting high acceptor concentrations achieved by *in-situ* arsenic doping

G. Kartopu[1,*], O. Oklobia[1], D. Turkay[2,3], D. R. Diercks[4], B. P. Gorman[4], V. Barrioz[5], S. Campbell[5], J. D. Major[6], M. K. Al Turkestani[7], S. Yerci[2,3,8], T. M. Barnes[9], N. S. Beattie[5], G. Zoppi[5], S. Jones[1], and S. J. C. Irvine[1]

[1] Centre for Solar Energy Research, OpTIC, St. Asaph Business Park, St. Asaph LL17 0JD, UK
[2] Centre for Solar Energy Research and Applications (GÜNAM), Middle East Technical University, 06800 Ankara, Turkey
[3] Department of Micro and Nanotechnology, Middle East Technical University, 06800 Ankara, Turkey
[4] George S. Ansell Department of Metallurgical and Materials Engineering, Colorado School of Mines, Golden, CO80401, USA
[5] Department of Mathematics, Physics and Electrical Engineering, Ellison Building, Northumbria University, Newcastle upon Tyne NE1 8ST, UK
[6] Stephenson Institute for Renewable Energy and Department of Physics, University of Liverpool, Liverpool, L69 7ZF, UK
[7] Department of Physics, Umm Al-Qura University, KSA, Mecca Al Taif Road, Mecca 24382, Saudi Arabia
[8] Department of Electrical and Electronics Engineering, Middle East Technical University, 06800 Ankara, Turkey
[9] National Renewable Energy Laboratory, 15013 Denver West Parkway, Golden, CO 80401, USA

Doping of CdTe using Group-V elements (As, P, and Sb) has gained interest in pursuit of increasing the cell voltage of CdTe thin film solar devices. Studies on bulk CdTe crystals have shown that much higher acceptor concentration than the traditional copper treatment is possible with As, P or Sb, enabled by high process temperature and/or rapid thermal quenching under Cd overpressure. We report a comprehensive study on *in-situ* As doping of poly-crystalline CdTe solar cells by MOCVD, whereby high acceptor densities, approaching 3×10^{16} cm^{-3} were achieved at low growth temperature of 390°C. No As segregation could be detected at grain boundaries, even for 10^{19} $As{\cdot}cm^{-3}$. A shallow acceptor level (+0.1 eV) due to As_{Te} substitutional doping and deep-level defects were observed at elevated As concentrations. Devices with variable As doping were analysed. Narrowing of the depletion layer, enhancement of bulk recombination, and reduction in device current and red response, albeit a small near infrared gain due to optical gap reduction, were observed at high concentrations. Device modelling indicated that the properties of the n-type window layer and associated interfacial recombination velocity are highly critical when the absorber doping is relatively high, demonstrating a route for obtaining high cell voltage.

Key words: CdTe; Group-V; doping; thin film; photovoltaics; MOCVD

* Corresponding author. E-mail: giray.kartopu@swansea.ac.uk

1. Introduction

Thin film CdTe solar cells have recently reached 22.1% conversion efficiency [1]. The nearly ideal short-circuit current density (J_{sc}) achieved with the record device (31.7 mA·cm^{-2}) has shifted attention to the open-circuit voltage (V_{oc}), in order to further reduce the deficit with the theoretical efficiency limit of ~30%. As a result, p-type doping of CdTe with Group-V elements (As, P, and Sb) has gained interest in recent years, which has been prompted by the shortcomings of the traditional copper (Cu) doping. In the latter process, a controlled amount of Cu is introduced into the absorber by annealing an ultra-thin (a few Å) copper film deposited on the back-surface of the CdTe absorber. Although high Cu incorporation and formation of substitutional Cu_{Cd} is possible under Te-rich conditions, the highest acceptor concentration (regardless of how much Cu used) is typically in the $10^{14} - 10^{15}$ cm^{-3} range [2,3]. This low active dopant level is due to severe self-compensation and grain boundary (GB) segregation effects [3], also limiting the minority carrier lifetime to ~1 ns [4]. Additionally, the fast diffusion of Cu within semiconductors can cause long-term device instability [5].

Substitution of Te sites with P or As under Cd-rich conditions combined with high growth temperatures is expected to result in shallow acceptor states with higher acceptor concentrations and longer minority carrier lifetimes compared to traditional Cu doping [6]. It is predicted through calculations that the relatively high formation energy of As (or P) interstitials should favour high rate of incorporation through As_{Te} (or P_{Te}) substitutional doping under Cd-rich growth conditions. However, formation of compensating AX centres through lattice-relaxation of the dopant element, leading to its conversion to a donor state [7], is likely to limit the hole density.

Recent efforts with As and P doping focused primarily on bulk CdTe crystals. Acceptor concentration of $10^{16} - 10^{17}$ cm^{-3} was achieved for As concentrations between $10^{16} - 10^{20}$ atom· cm^{-3} for single crystal CdTe [8]. The highest dopant activation efficiency was 40% for 1×10^{17} As·cm^{-3}, which rapidly reduced with increasing As concentration to below 1% for $>1\times10^{18}$ As·cm^{-3}. Photo-conductive behaviour of the samples was interpreted as evidence for the metastable AX centres and hence self-compensation. High temperature annealing followed by rapid quenching (~300°C/h) was seen to lead to high doping efficiencies (up to 80%); however, it was metastable and decayed rapidly to ~5%. Epitaxial CdTe:As layer growth was studied by molecular beam epitaxy under 20% Cd overpressure condition with Cd_3As_2 as the dopant source [9]. Nanometer-scale As-rich precipitates were observed to form and accompanied by degradation in crystal quality for $>7\times10^{18}$ As·cm^{-3}.

Group-V (P) and Group I (Cu, Na) doping introduced by post-growth diffusion were compared in single-, multi-, and poly-crystalline CdTe [10]. The multi-crystalline CdTe had

0.3-3 mm grains while poly-crystalline (px) films, by comparison, had grains of tens of microns in diameter. Group I (e.g. Cu) doping resulted in acceptor concentrations greater than 1×10^{16} cm^{-3} in bulk CdTe crystals and 10^{15} cm^{-3} in px film with only ~1 ns lifetime and poor doping stability. On the other hand, P doping for all samples produced greater than 1×10^{16} cm^{-3} acceptor concentration with 20-40 ns lifetime and high stability. Diffusion and doping efficiency of Group-V dopant elements As, P, and Sb in bulk-like px CdTe were studied by Colegrove *et al*. [11]. The px film was 20 μm thick containing 10-15 μm diameter CdTe grains. Although dopant segregation was also observed at the grain-boundaries, acceptor concentrations greater than 10^{16} cm^{-3} were obtained for As and P. Doping efficiency improved from 1% towards 3% following a post-diffusion Cd overpressure anneal.

Although device-like (superstrate) structures were fabricated in the latter studies [10,11] (e.g. for capacitance-voltage measurements) no photovoltaic (PV) activity was reported. It is therefore intriguing how a device-grade px CdTe thin films with smaller crystal grains (around 1 μm) could be effectively doped with Group-V elements and perform in a solar cell architecture.

In this study, behaviour of As doping in thin film px CdTe superstrate solar cell structures is systematically investigated using metal-organic chemical vapor deposition (MOCVD) to understand the role of Group V doping on CdTe PV devices. Doping during growth (*in-situ*) was preferred over post-deposition (*ex-situ*) methods to avoid grain-boundary segregation [12]. MOCVD is particularly suitable in controlled alloying of II-VI films [13] and introducing dopant reagents during growth. Prior to this work, *in-situ* As incorporated MOCVD CdTe thin films and solar cells were reported [14-17], but, to date, no detailed study was published on achievable acceptor densities and their correlation to photovoltaic (PV) properties. In the following sections, firstly the results with controlling the acceptor concentration in CdTe:As films will be presented. Secondly, the obtained solar cell characteristics for a range of selected p-type doping densities will be discussed with the aid of various spectroscopic data. Next, device modelling, performed to understand dependence of V_{oc} on doping and junction properties, will be presented to identify scope for higher performance solar cells featuring high acceptor concentration and high V_{oc}. Finally, defect levels formed within the CdTe bandgap as a result of As doping will be presented with linkage to the device characteristics, followed by discussions and overview.

2. Experimental section

2.1 CdTe:As thin film and solar cell deposition

A horizontal metalorganic chemical vapor deposition (MOCVD) reactor was used at atmospheric pressure to deposit the CdTe:As layers at 390°C. The organometallic precursors

were dimethylcadmium (DMCd), diisopropyltelluride (DiPTe) and tris-dimethylaminoarsine (tDMAAs) with hydrogen (H_2) as the carrier gas. All precursors used were adduct (high purity) grade supplied by various vendors. The partial pressure ratio DMCd/DipTe was varied between 2 to 4 to promote As incorporation into the growing CdTe layer under Cd-rich conditions. Thickness of the studied layers was 3 μm, which were deposited at ~0.7 $nm \cdot s^{-1}$ growth rate. The As concentration was controlled by tuning the tDMAAs flow between 1-3 sccm at a bubbler temperature of 18°C. Reference films with no intentional doping were also produced following heating and pumping down the As line and growth chamber to minimize the As memory. For the capacitance-voltage (*C-V*) measurements and to fabricate solar cells, n-type CdZnS counterparts were deposited onto transparent conducting oxide (TCO) coated glass substrates, while for Hall measurements an uncoated boro-aluminosilicate glass substrate was used. The CdZnS films were deposited at 360°C to a thickness of 0.15 μm using DMCd, diethylzinc, and ditertiarybutylsulphide (DtBS) organometallic precursors and H_2 carrier gas. Initial film composition was $Cd_{0.3}Zn_{0.7}S$, which altered to $Cd_{0.5}Zn_{0.5}S$ after full device processing, including the chlorine heat treatment (CHT) [18]. Reference CdS layers (for Hall measurements) were processed using DtBS and DMCd precursors at 315°C. TCO films (typically 4-8 Ohm sq. ITO) were surface-treated with an O_2 plasma prior to MOCVD which improves lateral uniformity. All solar cells, except for the reference (unintentionally doped) cell, also contained a 0.3 μm thick heavily As doped film as the back contact layer (BCL) for low ohmic resistance. The CHT process entailed deposition of a ~1 μm $CdCl_2$ layer at 200°C (using DMCd and tertiarybutylchloride precursors) on the back of the CdTe:As film and annealing the device structure at 420°C for 10 min in H_2 ambient. Deposition of CdZnS and CdTe as well as the CHT step were carried out sequentially and finally the sample was brought to room temperature at a cooling rate of ~300°C/h. A secondary device-activation anneal was also performed at 170°C for 90 min in air ambient, which reduces the barrier height at the back-contact and increases the acceptor concentration in the CdTe film by providing surface passivation [17,19]. Solar cells were completed by depositing eight gold (Au) squares of 0.5 × 0.5 cm by thermal evaporation on the treated CdTe surface. The front contact was formed using silver paste on a portion of the (exposed) TCO film surrounding the solar cells, i.e. Au contacts. A milder CHT entailing deposition of 0.5 μm $CdCl_2$ at 200°C followed by 3 min anneal at 420°C was applied to the reference CdZnS film to monitor the change in the donor density.

2.2 Characterization methods

As depth profiling was carried out via secondary ion-mass spectroscopy (SIMS) using a Cameca IMS-4f instrument with Cs+ ion source operating with 10 keV energy and 20 nA current at LSA Ltd. A ~1×1 cm specimen was cleaved and etched in 0.2% bromine solution (in methanol) to reduce surface roughness prior to SIMS measurements. Measurements were calibrated using a standard CdTe:As specimen prepared by ion-implantation. *C-V* characteristics were measured using a Solartron Impedance Analyzer at a frequency of 300 kHz using 10 mV ac bias amplitude. The Mott-Schottky equation was used to calculate the

acceptor density from the linear part of the C^{-2}-V curve around 0 V. In the rest of this paper, the term acceptor concentration will refer to the "free hole concentration" determined by the C-V analysis. This value for the bulk of CdTe absorber corresponds to the mean of the lower, flat part of the N_A-depth curves while depletion width (W_D) is the width of the flat portion. Film absorption (A) was calculated using transmittance (T) and reflectance (R) data, via the relationship $A = 1 - T - R$, which were collected in the 300 – 1100 nm range using a Bentham PVE300 spectral response system equipped with a halogen lamp (50-70 W) and calibrated using a Si photodetector. Reflectance measurements made use of an integrated sphere, in order to collect the diffused light. Hall conductivity measurements were carried out in dark using a magnetic field strength of 0.55T on the reference CdZnS and CdS films to obtain their donor density (N_D), carrier mobility (μ), and resistivity (ρ). Sample contacting for the Hall measurements comprised, thermal vapor deposition of 100 nm thick gold pads (each 1 mm diameter) on four corners of ~1×1 cm^2 thin film specimen on glass, contact-reinforcement by application of silver paste on the gold pads followed by oven curing at 150°C for 3 min and soldering with indium. All Hall samples also received the same air-anneal treatment at 170°C for 90 min as per the solar cell devices.

Specimen preparation for atom probe tomography (APT) analysis was completed using a lift-out method [20] in a FEI Helios 600i FIB/SEM instrument. TEM imaging of the specimens before and after APT analysis was performed in a FEI Talos F200X microscope using hardware capable of transfer between FIB, TEM, and APT instruments [21]. Laser pulsed APT analysis made use of a Cameca LEAP 4000X Si instrument at a laser pulse rate of 333 kHz, a laser pulse energy of 5.1 pJ, and a base temperature of 21.2K. The range of applied bias was 1600 – 4700 V. These conditions have been shown previously to result in ~50:50 measurement of Cd:Te [22]. The reconstruction was generated in Cameca's IVAS 3.6.12 software using the TEM image to inform the reconstruction parameters. For 1-D composition profiles, data were divided into 1 nm slices and the mass spectrum of each slice was quantified individually using a full-width $1/100^{th}$ maximum peak fitting criterion and local background subtraction. The overall mass spectrum from this specimen is available in the Atom Probe Tomography Mass Spectrum Database [23].

Light *J-V* curves were collected using an Abet Technologies Ltd. solar simulator with the light power density calibrated to AM1.5 using a GaAs reference cell. To study the back-contact barrier height and device parasitic resistances, temperature dependence of current-voltage (i.e. *JVT*) curves was measured in dark condition from ~50K to 300 K. EQE measurements were carried out using the Bentham PVE300 system under unbiased conditions. The system response was corrected by scanning the output of a c-Si reference detector.

A Horiba Jobin Yvon spectrometer was used for all photoluminescence (PL/TRPL)

measurements with a 1200 grooves/mm diffraction grating. Standard PL spectra were collected using a 532 nm continuous wave diode-pumped solid-state laser as an excitation source and collected using a CCD detector. The TRPL measurements used a pulsed laser diode excitation at 650 nm and the decay was collected with a picosecond photon detector. The decay signal for TRPL was selectively monitored at the peaks emerging near the CdTe bandgap energy.

Deep level transient spectroscopy (DLTS) analysis [24] was performed using a PhysTech FT1230 HERA DLTS system with a Linkam cryostat. Emission capacitance transients were recorded using reverse and pulse biases of 2V and 0V respectively with pulse durations in the range of 0.1-100ms depending on the sample. Three separate transient period widths of 19.2ms, 192ms and 480ms were measured with time constants related to emission being determined via correlator functions using a Fourier transform analysis method (DLFTS) [25]. Values for trap energy and capture cross section were derived from temperature dependent analysis of the trap emission time constants, τ_e, via the equation;

$$\tau_e = [(\sigma_p \nu_{th} N_V) e^{-\frac{E_T}{kT}}]^{-1} \quad (1)$$

where σ_p is the capture cross section for holes, E_T is the energy of the trap level (with respect to the valence band for holes), T is the temperature, N_V is the effective density of states in the valence band and v_{th} is the thermal velocity.

2.3 Device modelling

We utilized the optical and electrical device simulation tool, Silvaco ATLAS [26], for the numerical calculations. The effective density of states, carrier mobility, electron affinity and bandgap values of the ITO, CdZnS and CdTe layers are in accord with Refs. 27, 28 where the properties of the CdZnS layer was assumed to be similar to those of CdS. Surface recombination parameters for electrons (*Sn0*) and holes (*Sp0*) at the CdZnS/CdTe interface are assumed to be equal (i.e. *Sn0*/*Sp0* = 1). The Shockley-Read-Hall recombination lifetimes of electrons and holes in the CdTe absorber layer are both equal to 1 ns. The thicknesses of the ITO, CdZnS, and CdTe layers are 150 nm, 95 nm, and 3.3 μm, respectively. The $Cd_{1-x}Zn_xS$ and ITO layers are assumed to have a donor concentration of 1×10^{17} cm^{-3} and 1×10^{20} cm^{-3}, respectively. Electron and hole mobilities of 320 and 40 $cm^2 \cdot V^{-1} \cdot s^{-1}$, respectively, for the CdTe layer. These parameters are unchanged unless otherwise stated.

3. Results and Discussion

3.1. Doping efficiency

Dopant accumulation at the GBs is a serious problem in thin film solar cells [3,9]. Thus, it is important to find out whether the dopant atoms preferentially accumulate at grain boundaries of the px CdTe layer. We studied As distribution by atom probe tomography (APT) for high As concentrations between 10^{18} – 10^{19} As·cm^{-3}. Fig. 1 presents an exemplar APT result for 1×10^{19} As·cm^{-3} concentration. Transmission electron microscopy (TEM) imaging of the focussed ion beam-prepared specimen was used to confirm that a grain boundary was present in the field of view (Fig. 1a). Additionally, since this film was $CdCl_2$ treated prior to the measurements, Cl was used in the APT reconstruction to trace the grain boundary (GB), considering it tends to accumulate at GBs of CdTe [29,30]. It is clear that Cl indeed segregates but no As accumulation can be seen at the present GB even at high, 10^{18} – 10^{19} As·cm^{-3}, concentrations. However, As concentration showed some fluctuation from one grain to the next (see another example in Supplementary, Fig. S1).

The acceptor concentration (N_A) derived from *C-V* measurements for As concentrations ranging from ~1×10^{16} As·cm^{-3} to 1×10^{19} As·cm^{-3} is shown in Fig. 2. It can be seen that the N_A can be controlled within three decades from ~3×10^{13} to ~3×10^{16} cm^{-3}. The layers were grown under Cd-rich conditions, with a Cd/Te precursor ratio of 2 to facilitate As incorporation. Increasing this ratio to 4, the highest achievable N_A increased only marginally (from 2×10^{16} to 3×10^{16} cm^{-3}) with no noticeable change in the activation ratio. The depletion width (W_D) narrows with increasing N_A (or the As concentration), as can be expected from the relationship (valid for an abrupt junction whereby the dielectric constants of the p- and n-sides are equal)

$$W_D = \sqrt{\frac{2\varepsilon V_{bi}}{q}\left(\frac{1}{N_A} + \frac{1}{N_D}\right)} \quad (2)$$

where N_D is the donor density of n-type region (window layer), k the Boltzmann constant, ε the dielectric constant, q the electron charge, and V_{bi} the built-in potential [31]. The dielectric constant of the window and absorber materials (9.3 and 9.4, respectively) are assumed to be equal. A plot of N_A *vs.* W_D estimated from these profiles (Fig. 2 inset) confirms an inverse power dependence between the two parameters. Overall, these results show that px CdTe films with small grains can be effectively doped, similar to large CdTe crystals [11,12], using the *in-situ* MOCVD route.

3.2. Device characteristics

Four superstrate CdTe solar cells were prepared with the glass/TCO/CdZnS/CdTe:As/Au structure at selected As concentrations, covering the range of acceptor concentrations demonstrated in Sect. 3.1. The device structure is shown and described in detail by Fig. S2. The concentration of As in the bulk of the absorber, measured by secondary ion mass spectrometry (SIMS), is shown in Fig. 3a. The sample with 1×10^{16} As·cm^{-3} throughout was produced by unintentional doping (relying on the memory effect of As within the MOCVD

system) as a reference. Intentionally-doped samples exhibited bulk concentrations of 3×10^{17}, 4×10^{18} and 1×10^{19} As·cm^{-3}, which also shared a heavily-doped (~1×10^{19} As·cm^{-3}) thin CdTe back-contact layer (BCL) to avoid Schottky back contacts [14] dominating the PV forward bias characteristic. The acceptor concentration increased with As concentration whilst the doping efficiency, represented by activation ratio = N_A/[As], is below 1%, tending to decrease further with increasing As concentration (Fig. 3b). Light *J-V* curves (Fig. 3c) show that intentional As doping is essential for good device performance, with the lower concentration of 1×10^{16} As·cm^{-3} sample displaying poor cell parameters (see also Tab. 1). Among the intentionally-doped layers, the J_{sc} exhibited a gradual decrease with increasing As concentration while for 4×10^{18} As·cm^{-3}, the sample showed the best conversion efficiency (η) due to higher V_{oc} and *FF*. Temperature dependence of dark *J-V* curves was analysed (see Figs. S4-S5) to extract the back-contact barrier height (φ) and to observe the behaviour of series resistance (R_s) and shunt resistance (R_{sh}). It is found that $\varphi \approx 0.15$ eV for all intentionally As doped cells, which is considered not a limiting factor on the V_{oc} or the fill factor (*FF*) [32]. The R_{sh} showed degradation with increasing As concentration (especially at lower temperatures, see Fig. S5), suggesting increased recombination as the dopant concentration rises. Sample with 4×10^{18} As·cm^{-3} displayed the most favourable R_s and R_{sh}, commensurate with the high *FF*.

The low As activation ratio (<1%) combined with the contraction of W_D with N_A (Fig. 2 inset and Tab. 1) suggest that defect density and recombination within the non-depleted absorber bulk could rise with As concentration. Having a wide junction width and low density of excess (*non-activated*) dopant atoms (i.e. potential deep level traps) should be helpful for carrier collection. This effect can be clearly seen in the device external quantum efficiency (EQE) analysis (Fig. 4a), where the collection efficiency decreases at most visible wavelengths and the slope at long wavelengths (< 820 nm) increases with increasing As concentration. Thus, the best J_{sc} obtained for the 3×10^{17} As·cm^{-3} device appears to be linked to lower bulk recombination enabled by its relatively wide depletion width and lower non-active As concentration. On the other hand, despite having the largest W_D, the 1×10^{16} As·cm^{-3} device displays a buried junction behaviour [33] indicating insufficient acceptors for most of the film depth. Overall, it can be assumed that sufficient acceptor concentration ($N_A > \sim10^{14}$ cm^{-3}) is essential for good device operation, while the optimum doping is just over 1×10^{18} As·cm^{-3} with $N_A \approx 1\times10^{16}$ cm^{-3}.

Another notable feature in the long wavelength EQE response is the development of a shoulder in the near infrared (850 - 950 nm) region with increasing acceptor concentration [34] (see inset to Fig. 4a). To elucidate this effect, we carried out optical (absorption and photoluminescence, PL) measurements. The absorption spectra (Fig. 4b) confirm a gradual increase in absorption towards infrared, in good agreement with the stepwise enhancement in device infrared spectral response observed with increasing As concentration. The PL spectrum of the low-doped (1×10^{16} As·cm^{-3}) specimen features two emission bands, at 830

and 860 nm (Fig. 4c). The former can be linked to direct-bandgap transition in CdTe and the latter to S diffusion, i.e. CdS_xTe_{1-x} phase close to the interface to the window layer [4,35]. When the As concentration is increased to 3×10^{17} As·cm^{-3}, in addition to the 830 and 860 nm emission bands a tail develops towards the infrared. With further increase of the As concentration, the 830 and 860 nm emission bands weaken while the intensity, position, and width of the infrared emission increase, resulting in the emergence of a new peak at 880 (900) nm for the 4×10^{18} (1×10^{19}) As·cm^{-3} concentration. The gradual redshift, broadening, and relative enhancement of the infrared emission suggest that the optical gap of CdTe reduces with As concentration, in accord with the absorption data. This effect could be due to band-tailing, where a shallow acceptor state is predicted to form at 60-100 meV above the valence band edge (E_v) due to As_{Te} substitution. This value is commensurate with the literature, which reports the activation energy of an arsenic atom occupying a Te site as an acceptor to be 55–90 meV [16,36,37].

To deduce the minority carrier lifetime in the bulk of CdTe:As layer, time-resolved PL (TRPL) measurements were carried out by exciting the solar cell structures through the glass side. The absorption depth of the laser (650 nm wavelength) in CdTe is around ~200 nm considering the absorption constant of CdTe at this wavelength, while in this region the glass/ITO/CdZnS front stack is virtually transparent. Therefore, the PL signal originates within the CdTe layer close to the CdZnS/CdTe interface. A two-exponential fit was applied to the PL decay curves in Fig. 5 which gave the lifetimes τ_1 and τ_2 (inset to Fig. 5). τ_1, obtained near $t \approx 0$ s, is shorter and usually related to charge separation (drift/diffusion); τ_2 is due to carrier recombination and can be used to track the minority carrier lifetime [4,38]. Both lifetimes increase with As concentration increasing from 1×10^{16} to 3×10^{17} As·cm^{-3}, and then reduce slightly to a saturated level for higher doping (4×10^{18} and 1×10^{19} As·cm^{-3}). This is similar to the observations with Cu doping of CdTe. Cu_{Cd} was observed to increase lifetime at low concentration, attributed to replacement of defects such as Te_{Cd} or cadmium vacancies (V_{Cd}) as observed in PL spectra [39]. At large Cu concentrations, however, the lifetime was observed to decrease, which appeared to be linked in with increased recombination centre density introduced by Cu in the CdTe layer [40]. Among our CdTe:As samples, the longest minority lifetime (~3 ns) is observed for 3×10^{17} As·cm^{-3}. Combined with the relatively large W_D of this sample (Tab. 1), this suggests that the charge collection should be better than the devices with higher As concentrations. This is indeed the case as evidenced by the observation of the highest J_{sc} and EQE values for this device. On a further note, for samples with large surface recombination velocity (S), the instantaneous lifetime (τ_1) is

$$\tau_1 \approx (\alpha S)^{-1} \tag{3}$$

where α is the absorption coefficient of CdTe at the excitation wavelength [41]. Accordingly, using $\tau_1 = 0.6 - 1.0$ ns (Fig. 5 inset) we obtain $S = 2\times10^4$ to 3×10^4 cm·s^{-1} for the current set of CdTe:As devices.

3.3. Device modelling

As can be seen in Fig. 3b and Tab. 1, the acceptor density in the absorber of the CdZnS/CdTe solar cells can be controlled up to 2×10^{16} cm^{-3}. The V_{oc} rises by ~35 mV as the N_A is increased from 3×10^{14} to 1×10^{16} cm^{-3}, and then it decreases by ~20 mV with a further increase to 2×10^{16} cm^{-3}. This trend is counterintuitive since significantly greater voltage gains would be predicted if the V_{oc} was controlled purely by the N_A. Following the relationship [42]

$$\Delta V_{oc} \approx (kT/q)\ln\,(N_{A1}/N_{A2}) \quad (4)$$

where N_{A1} and N_{A2} correspond to acceptor densities in two different cells, it is expected that the respective V_{oc} increments should have been 88 and 17 mV, respectively. Therefore, it is clear that for these solar cells, the V_{oc} is also influenced by increased recombination for high acceptor concentration.

It is curious whether the high acceptor concentration achieved in CdTe:As devices would have negative implications on recombination characteristics. To this end, device simulations were carried out, which revealed the increasing importance of surface recombination and band alignment at the absorber/window interface as a result of having an absorber with high acceptor concentration. Ways to suppress this recombination were then investigated for obtaining higher V_{oc} devices.

The sensitivity of V_{oc} to the changing surface recombination velocity (S) is depicted in Fig. 6 for three different N_A values and conduction band offsets (CBO) between CdZnS and CdTe, determined by their electron affinity (χ), i.e. $\Delta E_c = \chi_{CdTe} - \chi_{CdZnS}$. Since all the electrical parameters are kept the same, these cases also represent varying work function differences between the two layers, and hence varying strengths of band bending and inversion on the absorber side. For a negative CBO (Fig. 6a) or a negligible work function difference (Fig. 6b) V_{oc} becomes highly sensitive to surface recombination for higher N_A values of 1×10^{16} and 2×10^{16} cm^{-3}. However, in the presence of positive CBO, as in Fig. 6c, for each doping concentration, V_{oc} is approximately insensitive to the surface recombination. In other words, the benefit of having a high N_A (>10^{16} cm^{-3}) for improved V_{oc} would be lost when S is high ($\geq 10^3$ - 10^4 cm·s^{-1}) and CBO is negative or close to zero. In these cases, the V_{oc} for $N_A = 2\times10^{16}$ cm^{-3} can in fact reduce below that of $N_A = 1\times10^{16}$ cm^{-3}, as also observed experimentally (Tab. 1). The critical S value at which this occurs reduces from $1\text{-}2\times10^4$ to $3\text{-}4\times10^3$ cm·s^{-1} as the CBO reduces from 0 to -0.15 eV.

By comparing the experimental data (*viz.* $S = 2\text{-}3\times10^4$ cm·s^{-1}, and the V_{oc} loss of ~20 mV observed when N_A is increased from 1×10^{16} to 2×10^{16} cm^{-3}) with the simulation data (Fig. 6), we estimate the experimental CBO between CdZnS and CdTe to be close to 0 eV. This is relatively favourable compared to a CBO of -0.1 eV measured for the CdS/CdTe junction

[43], and explains why the V_{oc} improved by 60-70 mV when the CdS layer is substituted with CdZnS for CdTe:As cells in a previous study [13]. We also investigated the influence of window layer thickness and its doping (donor) density N_D on the V_{oc} for 10^{14} – 10^{17} cm^{-3} acceptor concentrations in the absorber layer. To enhance the impact of window layer parameters, a low CBO of –0.15 eV and high S of 10^4 cm·s^{-1} were selected. Although the window layer thickness appeared to have a minimal effect for thicknesses greater than 20 nm (not shown), N_D is found to have a substantial influence (Fig. 7). Accordingly, when N_A is greater than 1×10^{16} cm^{-3}, window layer doping must exceed 1×10^{18} cm^{-3} to access high V_{oc} values. This observation stems from the fact that interfacial recombination would increase substantially when the electron and hole concentrations (n_s and p_s, respectively) at the window/absorber interface are at a balance, namely $n_s \approx p_s$, provided the surface recombination parameters for holes and electrons are nearly equal, i.e. $S_{n0} \approx S_{p0}$. For CBO ≈ 0 eV and a sufficiently thick n-type window layer, this condition is met easily when $N_A \approx N_D$; in other words, to suppress surface recombination a n^+p or p^+n type one-sided junction would be favourable. Comparing experimental data shown in Fig. 2 inset with Eq. 2 (see Fig. S3) we estimate $N_D \approx 1\times10^{16}$ cm^{-3} for the CdZnS film (supported by Hall data on reference CdZnS single layer, Tab. S1), which suggests that the surface recombination will dominate with a comparable N_A of ~1×10^{16} cm^{-3}.

3.4. Defect states

Deep level transient spectroscopy (DLTS) was used to characterise the defects in CdTe:As layers of the reported solar cells. DLTS measures the capacitance transient of a reverse biased p^+n or n^+p junction due to carrier injection. A DLTS spectrum is obtained by plotting the change in capacitance, ΔC, through a temporal rate window (Δt) versus temperature, T. Fig. 8 shows recorded DLTS spectra for CdTe:As samples with varied doping levels in the 125-375K range. The positive peaks in the DLTS signal represent majority (hole) traps in a p-type material. Trap energy levels and capture cross sections, extracted from Arrhenius plots of trap emission time constant, τ_e, as a function of temperature are shown in Fig. 9 with values summarized in Tab. 2. All trap energies are given as energy above the valence band edge.

In order to identify the role of As doping in CdTe, it is useful to first consider the defect spectra observed for the unintentionally-doped sample, having the lowest As concentration of 1×10^{16} As·cm^{-3}, in Fig. 8a. The low cell efficiency of this sample, 0.2%, meant the signal extracted by the DLTS system was particularly low and peaks were only resolvable by using a particularly long pulse width of 100 ms. Despite the difficulty of the measurement, two hole-trap states, H1 and H2 were clearly resolved. H1 has a trap energy in the range 234-284 meV with a capture cross section in the 10^{-17} – 10^{-18} cm^2 range, whilst H2 is a mid-gap state at 667-692 meV with ~10^{-15} cm^2 capture cross section. As H1 and H2 are observable in all samples, these levels are likely related to: (a) native defects, (b) some aspect of device production which is common to all samples, such as chlorine treatment or hydrogen

incorporation, or (c) inter-diffusion at the interface with the window layer [35,44]. The specific source of these defects is difficult to discern as large numbers of defects have previously been identified at similar energetic positions with various techniques and with varied designations. However, this study differs from most of the literature which studied CdTe doping with Cu primarily under Te-rich conditions [45,46]. Here, Cd interstitials (Cd_i), tellurium vacancies (V_{Te}) and Cd antisite (Cd_{Te}) native defects instead can be anticipated under Cd-rich conditions [47]. It is therefore likely that these native defects and other complexes involving Cl or H are responsible for the appearance of peaks H1 and H2.

For samples with higher As concentration an additional level, labelled H3, not present in the unintentionally-doped sample, is visible in the DLTS spectra. This level is somewhat masked in the lower-doped sample 3×10^{17} As·cm^{-3}, Fig. 8b, but becomes visible for 4×10^{18} As·cm^{-3} (Fig. 8c) then gains intensity in the heavily (1×10^{19} As·cm^{-3}) doped sample, Fig. 8d. Arrhenius analysis gives a comparatively wide energy range for this level of 438-595 meV, with the trap being shallowest in the highest efficiency sample 4×10^{18} As·cm^{-3} and deepest for the highest 1×10^{19} As·cm^{-3} concentration. For high As doping, we were also able to identify an additional shallow level at 116-121 meV (H4), Fig. 8c inset, by using a lower temperature range 80-200K and a rapid 1 µs filling pulse. This level is shallow enough to be an effective acceptor state, e.g. As_{Te} (in accord with the PL data and related literature [16,36,37], see Sect. 3.2), and is the source of increased acceptor concentration observed for As-doped samples. In contrast, the increasing depth of the H3 defect level for higher doping may be linked to the decrease in efficiency when 1×10^{19} As·cm^{-3} concentration is used. DFT calculations predict a deep trap state resulting from the AX centre or a V_{Cd}-As_{Te} complex with a value of 396 meV [37]. Here the trap state observed is deeper and with a broad range up to 595 meV, however assessment could be slightly skewed towards larger energy by the close proximity of the H2 level. V_{Cd} is unlikely to have formed, considering the Cd-rich condition and since doping efficiency is below 1% for all samples, As dopants are highly compensated; thus, it is meaningful to attribute the H3 level to AX centre formation, which is a deep donor state. Alternatively, As_{Te} complexing with some H- or Cl-related centre could also be an appropriate explanation for this H3 level. Additionally, the H2 level appears to weaken for the heavy doping (Fig. 8d), which suggest that the defect responsible for this level is partially eliminated (or converted to another defect type) with high As incorporation. The deeper defect levels (H2 and H3) can be linked with increased bulk recombination observed with heavy As incorporation through reduction in the minority carrier lifetime and poor carrier collection for long wavelength absorption. Self-compensation through AX centres (H3 level) is also likely to limit the acceptor concentration (N_A) and the doping efficiency.

3.5. Discussion

Our data are commensurate with recent theoretical reports. Song *et al*. showed that a positive CBO = +0.1-0.3 eV at the absorber/window layer interface would help to suppress

surface recombination [48]. For $N_A = 2\times10^{15}$ cm^{-3} and CBO = +0.2 eV, they predict a V_{oc} of 840 mV (915 mV) when the bulk lifetime is 0.5 ns (10 ns). Kanevce *et al*. investigated key parameters to improve the solar cell efficiency to over 25% by achieving V_{oc} greater than 1000 mV and N_A as high as 2×10^{16} cm^{-3} [49]. Their simulations also showed a small positive CBO around +0.1 eV is helpful to suppress the interfacial recombination when S is as large as 10^5 cm·s^{-1}. However, to really push the V_{oc} above the 1000 mV limit, desirable parameters established are: $S \approx 100$ cm·s^{-1}, bulk minority carrier lifetime ~100 ns and CdTe grains > 5 μm. If CdTe grains were as large as 20 μm then a bulk lifetime of ~1 ns would be tolerable for high V_{oc} with such a surface recombination value. In other words, *both* interface and bulk properties must be improved to suppress recombination losses in order to materialize the benefit of having a high N_A absorber. Reduction of surface recombination velocity from ~10^5 to 100 cm·s^{-1} has recently been measured for px Cd(Se)Te films when using Al_2O_3 passivation layers [50]. Long bulk minority carrier lifetimes (up to tens of ns) with $V_{oc} > 900$ mV were measured in single crystal CdTe and CdZnTe devices [51]. Increasing the grain size of px CdTe films from 1 to 7 μm is shown to be equivalent to decreasing grain- boundary recombination velocity by three orders of magnitude, with large high- quality grains enabling CdTe lifetimes over 50 ns [52]. These promising observations provide motivation and directions to future efforts in obtaining CdTe solar cells featuring both high N_A and V_{oc}.

4. Conclusions

High acceptor concentration exceeding 10^{16} cm^{-3} is achieved in px CdTe thin films with small grains (submicron diameter) using a Group V (As) impurity via *in-situ* doping by MOCVD. No As segregation at grain boundaries but small grain-to-grain fluctuations in dopant concentration were observed. The depletion width was inversely proportional to the acceptor concentration, as $N_A \propto W_D^{-0.33}$. The doping efficiency was limited to ~1%. Solar cells made from selected As concentrations, leading to acceptor concentration between ~10^{13} and 2×10^{16} cm^{-3}, exhibited several remarkable signatures in EQE and V_{oc} behaviour. Acceptor concentration greater than 10^{14} cm^{-3} was found essential for good device operation with low series resistance. The best spectral response was observed for ~3×10^{17} cm^{-3} As concentration ($N_A \approx 3\times10^{14}$ cm^{-3}), displaying the highest EQE and J_{sc} values. For higher dopant concentrations, the red response degraded gradually, reducing the J_{sc}, in relation to enhanced bulk recombination. The contraction of W_D towards the window layer interface, the reduction in minority carrier lifetime, and the increase in number and density of defects were considered responsible for the enhanced bulk recombination. Interestingly, increasing As concentration also led to enhanced optical absorption with a small EQE/J_{sc} gain in the infrared due to band tailing. The best cell performance was obtained near 4×10^{18} As·cm^{-3} (with $N_A \approx 1\times10^{16}$ cm^{-3}) due to V_{oc} and *FF* being at their optimum. When the As doping was raised to 1×10^{19} cm^{-3} ($N_A \approx 2\times10^{16}$ cm^{-3}) all device parameters showed degradation.

Device simulations revealed the importance of surface recombination at the interface to the window layer on V_{oc} losses for solar cells with high acceptor concentration and high

surface recombination velocities ($\geq 10^4$ cm·s^{-1}). It is shown that a small positive conduction band offset (around +0.15 eV) and high donor density ($N_D > 10^{18}$ cm^{-3}) in the window layer, resulting in a n^+p type junction, would mitigate the surface recombination related V_{oc} losses when the N_A of the absorber is as high as obtained in this work. Further efforts to decrease the surface recombination, e.g. by using a passivation layer at the hetero-interface, and increasing the bulk lifetime towards 10 ns, e.g. by increasing the CdTe grain size, would be needed to increase the V_{oc} of px CdTe solar cells towards 1000 mV. This study forms a solid understanding to Group V doping and related device characteristics of px CdTe solar cells with high acceptor concentration and illustrates the obstacles and possible routes to achieving high V_{oc}.

Acknowledgements

The authors would like to acknowledge funding by the European Regional Development Fund through the Solar Photovoltaic Academic Research Consortium (SPARC II) operated by the Welsh Government and from the Engineering and Physical Sciences Research Council (EPSRC) via grants EP/N024389/1 and the North East Centre for Energy Materials (EP/R021503/1). We thank Sachit Grover, at First Solar, Inc. for fruitful discussions and provision of the cross-sectional scanning electron microscopy image of our solar cells.

References

1 First Solar press release, "First Solar Achieves Yet Another Cell Conversion Efficiency World Record", 23 February 2016, http://investor.firstsolar.com/news-releases/news-release-details/first-solar-achieves-yet-another-cell-conversion-efficiency.

2 J.D. Major, Y.Y. Proskuryakov, and K. Durose, Impact of CdTe surface composition on doping and device performance in close Space sublimation deposited CdTe solar cells, Prog. Photovolt. 21 (2013) 436-443.

3 J. Perrenoud, L. Kranz, C. Gretener, F. Pianezzi, S. Nishiwaki, S. Buecheler, and A. N. Tiwari, A comprehensive picture of Cu doping in CdTe solar cells, J. Appl. Phys. 114 (2013) 174505.

4 D. Kuciauskas, A. Kanevce, J. N. Duenow, P. Dippo, M. Young, J. V. Li, D. H. Levi, and T. A. Gessert, Spectrally and time resolved photoluminescence analysis of the CdS/CdTe interface in thin-film photovoltaic solar cells, Appl. Phys. Lett. 102 (2013) 173902.

5 J. Ma and S.-H. Wei, Origin of Novel Diffusions of Cu and Ag in Semiconductors: The Case of CdTe, Phys. Rev. Lett. 110 (2013) 235901.

6 J.H. Yang, W.J. Yin, J.S. Park, J. Burst, W.K. Metzger, T. Gessert, T. Barnes, S.H. Wei, Enhanced p-type dopability of P and As in CdTe using non-equilibrium thermal processing, J. Appl. Phys. 118 (2015) 025102.

7 A. Nagaoka, D. Kuciauskas, J. McCoy, and M. A. Scarpulla, High p-type doping, mobility, and photocarrier lifetime in arsenic-doped CdTe single crystals, Appl. Phys. Lett. 112 (2018) 192101.
8 A. Nagaoka, D. Kuciauskas, and M. A. Scarpulla, Doping properties of cadmium-rich arsenic-doped CdTe single crystals: Evidence of metastable AX behaviour, Appl. Phys. Lett. 111 (2017) 232103.
9 G.L. Burton, D.R. Diercks, O.S. Ogedengbe, P.A.R.D. Jayathilaka, M. Edirisooriya, T.H. Myers, K.N. Zaunbrecher, J. Moseley, T.M. Barnes, B.P. Gorman, Understanding arsenic incorporation in CdTe with atom probe tomography, Sol. Energy Mat. Sol. Cells 182 (2018) 68-75.
10 J.M. Burst, S.B. Farrell, D.S. Albin, E. Colegrove, M.O. Reese, J.N. Duenow, D. Kuciauskas, and Wyatt K. Metzger, Carrier density and lifetime for different dopants in single-crystal and polycrystalline CdTe, APL Mater. 4 (2016) 116102.
11 E. Colegrove, J.-H. Yang, S.P. Harvey, M.R. Young, J.M. Burst, J.N. Duenow, D.S. Albin, S.-H. Wei, and W K Metzger, Experimental and theoretical comparison of Sb, As, and P diffusion mechanisms and doping in CdTe, J. Phys. D: Appl. Phys. 51 (2018) 075102.
12 B. E. McCandless, W.A. Buchanan, C.P. Thompson, G. Sriramagiri, R.J. Lovelett, J. Duenow, D. Albin, S. Jensen, E. Colegrove, J. Moseley, H. Moutinho, S. Harvey, M. Al-Jassim, and W.K. Metzger, Overcoming Carrier Concentration Limits in Polycrystalline CdTe Thin Films with In Situ Doping, Sci. Rep. 8 (2018) 14519.
13 G. Kartopu, A.J. Clayton, W.S.M. Brooks, S.D. Hodgson, V. Barrioz, A. Maertens, D.A. Lamb, S.J.C. Irvine, Effect of window layer composition in $Cd_{1-x}Zn_xS$/CdTe solar cells, Prog. Photovolt. 22 (2014) 18-23.
14 S.J.C. Irvine, V. Barrioz, D. Lamb, E.W. Jones, and R.L. Rowlands-Jones, MOCVD of thin film photovoltaic solar cells—Next-generation production technology?, J. Cryst. Growth, 310 (2008) 5198–5203.
15 W.S.M. Brooks, S.J.C. Irvine, V. Barrioz, and A.J. Clayton, Laser beam induced current measurements of $Cd_{1-x}Zn_xS$/CdTe solar cells, Sol. Energy Mat. Sol. Cells, 101 (2012) 26–31.
16 Y.Y. Proskuryakov, K. Durose, J.D. Major, M.K. AlTurkestani, V. Barrioz, S.J.C. Irvine, E.W. Jones, Doping levels, trap density of states and the performance of co-doped CdTe (As,Cl) photovoltaic devices, Sol. Energy Mat. Sol. Cells 93 (2009) 1572-1581.
17 S.L. Rugen-Hankey, A.J. Clayton, V. Barrioz, G. Kartopu, S.J.C. Irvine, J.D. McGettrick, D. Hammond, Improvement to thin film CdTe solar cells with controlled back surface oxidation, Sol. Energy Mat. Sol. Cells 136 (2015) 213–217.
18 G. Kartopu, A.A. Taylor, A.J. Clayton, V. Barrioz, D.A. Lamb, and S.J.C. Irvine, $CdCl_2$ treatment related diffusion phenomena in $Cd_{1-x}Zn_xS$/CdTe solar cells, J. Appl. Phys. 115 (2014) 104505.
19 G. Kartopu, L.J. Phillips, V. Barrioz, S.J.C. Irvine, S.D. Hodgson, E. Tejedor, D. Dupin, A.J. Clayton, S.L. Rugen-Hankey, and K. Durose, Progression of metalorganic chemical vapour-deposited CdTe thin-film PV devices towards modules, Prog. Photovolt. 24 (2016) 283-291.

20 K. Thompson, D. Lawrence, D.J. Larson, J.D. Olson, T.F. Kelly, and B. Gorman, In situ site-specific specimen preparation for atom probe tomography, Ultramicroscopy 107 (2007) 131-139.
21 B.P. Gorman, D. Diercks, N. Salmon, E. Stach, G. Amador, and C. Hartfield, Hardware and techniques for cross-correlative TEM and atom probe analysis, Microscopy Today 16 (2008) 42-47.
22 D.R. Diercks, and B.P. Gorman, Nanoscale measurement of laser-induced temperature rise and field evaporation effects in CdTe and GaN, J. Phys. Chem. C 119 (2015) 20623-20631.
23 D.R. Diercks, B.P. Gorman, and S.S. Gerstl, An Open-Access Atom Probe Tomography Mass Spectrum Database, Microscopy and Microanalysis 23 (2017) 664-665.
24 A.R. Peaker, V. P. Markevich, and J. Coutinho, Tutorial: Junction spectroscopy techniques and deep-level defects in semiconductors, J. Appl. Phys. 123 (2018) 161559.
25 S. Weiss, and R. Kassing, Deep Level Transient Fourier Spectroscopy (DLTFS)—A technique for the analysis of deep level properties, Solid. State. Electron. 31 (1988) 1733–1742.
26 "Atlas User's Manual." www.silvaco.com.
27 T. Minami, T. Miyata, and T. Yamamoto, Work function of transparent conducting multicomponent oxide thin films prepared by magnetron sputtering, Surf. Coatings Technol. 108–109 (1998) 583–587.
28 M. Gloeckler, A. L. Fahrenbruch, and J. R. Sites, Numerical Modeling of CIGS and CdTe Solar Cells: Setting the Baseline, Proc. 3rd World Conference of Photovoltaic Energy Conversion 1 (2003) 491–494.
29 C. Li, Y. Wu, J. Poplawsky, T.J. Pennycook, N. Paudel, W. Yin, S.J. Haigh, M.P. Oxley, A.R. Lupini, M. Al-Jassim, S.J. Pennycook, and Y. Yan, Grain-Boundary-Enhanced Carrier Collection in CdTe Solar Cells, Phys. Rev. Lett. 112 (2014) 156103.
30 J.D. Major, Grain boundaries in CdTe thin film solar cells: a review Semicond. Sci. Technol. 31 (2016) 093001.
31 S.M. Sze, and Kwok K. Ng, Semiconductor Devices Physics and Technology, John Wiley & Sons, New York, 3rd Edition (2007) p.83.
32 A.L. Fahrenbruch, Exploring Back Contact Technology to Increase CdS/CdTe Solar Cell Efficiency, Proc. Mater. Res. Soc. Meeting (2007) DOI: 10.1557/PROC-1012-Y07-05.
33 J.D. Major, K. Durose, Study of buried junction and uniformity effects in CdTe/CdS solar cells using a combined OBIC and EQE apparatus, Thin Solid Films 517 (2009) 2419-2422.
34 S. Grover, X. Li, W. Zhang, M. Yu, G. Xiong, M. Gloeckler, and R. Malik, Characterization of Arsenic Doped CdTe Layers and Solar Cells, IEEE 44th Photovoltaic Specialist Conference (2017) 1193-1195.
35 A.A. Taylor, J.D. Major, G. Kartopu, D. Lamb, J. Duenow, R.G. Dhere, X. Maeder, S.J.C. Irvine, K. Durose, B.G. Mendis, A comparative study of microstructural

stability and sulphur diffusion in CdS/CdTe photovoltaic devices, Sol. Energy Mat. Sol. Cells 141 (2015) 341-349.
36 M. Ekawa, K. Yasuda, T. Ferid, M. Saji, and A. Tanaka, Mechanism of arsenic incorporation and electrical properties in CdTe layers grown by metalorganic vapor phase epitaxy, J. Appl. Phys. 71 (1992) 2669-2674.
37 T. Ablekim, S.K. Swain, W.-J. Yin, K. Zaunbrecher, J. Burst, T.M. Barnes, D. Kuciauskas, S.-H. Wei, and K.G. Lynn, Self-compensation in arsenic doping of CdTe, Sci. Rep. 7 (2018) 4563.
38 A. Kanevce, D. H. Levi, and D. Kuciauskas, The role of drift, diffusion, and recombination in time- resolved photoluminescence of CdTe solar cells determined through numerical simulation, Prog. Photovolt. 22 (2014) 1138-1146.
39 T. A. Gessert, W. K. Metzger, P. Dippo, S. E. Asher, R. G. Dhere, and M. R. Young, Dependence of carrier lifetime on Cu-contacting temperature and ZnTe:Cu thickness in CdS/CdTe thin film solar cells, Thin Solid Films 517 (2009) 2370-2373.
40 S.H. Demtsu, D.S. Albin, J.R. Sites, W.K. Metzger, A. Duda, Cu-related recombination in CdS/CdTe solar cells, Thin Solid Films 516 (2008) 2251-2254.
41 R.K. Ahrenkiel and S.W. Johnston, An optical technique for measuring surface recombination velocity, Sol. Energy Mat. Sol. Cells 93 (2009) 645-649.
42 T. Nakada, Invited Paper: CIGS-based Thin Film Solar Cells and Modules: Unique Material Properties, Mater. Lett. 8 (2012) 179-185.
43 B. Siepchen, H.-J. Schimper, A. Klein, and W. Jaegermann, XPS studies of single crystalline CdTe/CdS interfaces, J. Electron Spectrosc. Relat. Phenom. 190 (2013) 54–63.
44 D. Krasikov, and I. Sankin, Defect interactions and the role of complexes in the CdTe solar cell absorber, J. Mater. Chem. A 5 (2017) 3503-3513.
45 T.A. Gessert, S.-H. Wei, J. Ma, D.S. Albin, R.G. Dhere, J.N. Duenow, D. Kuciauskas, A. Kanevce, T.M. Barnes, J.M. Burst, W.L. Rance, M.O. Reese, H.R. Moutinho, Research strategies toward improving thin-film CdTe photovoltaic devices beyond 20% conversion efficiency, Sol. Energy Mat. Sol. Cells 119 (2013) 149-155.
46 V. Komin, B. Tetali, V. Viswanathan, S. Yu, D.L. Morel, and C.S. Ferekides, The effect of the $CdCl_2$ treatment on CdTe/CdS thin film solar cells studied using deep level transient spectroscopy, Thin Solid Films 431-432 (2003) 143-147.
47 V. Babentsov, V. Corregidor, K. Benz, M. Fiederle, T. Feltgen, and E. Dieguez, Defect engineering in CdTe, based on the total energies of elementary defects, Nucl. Instr. Meth. Phys. Res. A 458 (2001) 85-89.
48 T. Song, A. Kanevce, and J. R. Sites, Emitter/absorber interface of CdTe solar cells, J. Appl. Phys. 119 (2016) 233104.
49 A. Kanevce, M. O. Reese, T. M. Barnes, S. A. Jensen, and W. K. Metzger, The roles of carrier concentration and interface, bulk, and grain-boundary recombination for 25% efficient CdTe solar cells, J. Appl. Phys. 121 (2017) 214506.
50 D. Kuciauskas, J.M. Kephart, J. Moseley, W.K. Metzger, W.S. Sampath, and P. Dippo, Recombination velocity less than 100 cm/s at polycrystalline Al_2O_3/CdSeTe interfaces, Appl. Phys. Lett. 112 (2018) 263901.

51 J.N. Duenow, J.M. Burst, D.S. Albin, M.O. Reese, S.A. Jensen, S.W. Johnston, D. Kuciauskas, S.K. Swain, T. Ablekim, K.G. Lynn, A.L. Fahrenbruch, and W.K. Metzger, Relationship of Open-Circuit Voltage to CdTe Hole Concentration and Lifetime, IEEE Journal of Photovoltaics 6 (2016) 1641-1644.

52 M. Amarasinghe, E. Colegrove, J. Moseley, H. Moutinho, D. Albin, J. Duenow, S. Jensen, J. Kephart, W. Sampath, S. Sivananthan, M. Al- Jassim, and W.K. Metzger, Obtaining Large Columnar CdTe Grains and Long Lifetime on Nanocrystalline CdSe, MgZnO, or CdS Layers, Adv. Ener. Mater. 8 (2018) 1702666.

Tables.

Table 1 Typical *C-V* and *J-V* parameters of CdZnS/CdTe solar cells for various As concentrations.

$[As]_{bulk}$ (cm^{-3})	N_A (cm^{-3})	W_D (μm)	J_{sc} ($mA \cdot cm^{-2}$)	V_{oc} (mV)	FF (%)	η (%)
1×10^{16}	7×10^{13}	1.20	1.0	464	46	0.2
3×10^{17}	3×10^{14}	0.75	24.0	730	65	11.4
4×10^{18}	1×10^{16}	0.23	23.2	763	75	13.3
1×10^{19}	2×10^{16}	0.18	22.1	742	74	12.1

Table 2 Trap energy levels (E_T) and capture cross sections (σ) of main defects observed in DLTS spectra of CdTe:As samples

Peak	**E_T (meV)**	**σ (cm^2)**	**Assignment**
H1	234-284	$(0.37\text{-}4.14) \times 10^{-18}$	Native defect and/or Cl or H related complex (Cd-rich growth)
H2	667-692	$(1.47\text{-}9.09) \times 10^{-15}$	Native defect and/or Cl or H related complex (Cd-rich growth)
H3	438-595	$(0.19\text{-}1.61) \times 10^{-14}$	AX center and/or As_{Te} related complex (donor)
H4	116-121	$(4.31\text{-}6.84) \times 10^{-14}$	As_{Te} (shallow acceptor)

Figure Captions.

Fig. 1 A needle-shaped APT px CdTe specimen, exhibiting two grains and a GB, as imaged by TEM **(a)**. The APT reconstruction **(b)** shows a 0.9 at% Cl surface (yellow) and a 97.6 at% Cd+Te surface (black), which highlights the GB location, and the region that was used for the 1-D atomic concentration profiles of elements Cd, Te, Cl, and As **(c)** in the direction of the blue arrow in (b), derived from APT. No As accumulation, but Cl segregation can be seen around the GB. The dashed line is the mean value of As present in the region of interest.

Fig. 2 Acceptor concentration (N_A) profile for px CdTe samples produced by *in-situ* doping with As concentration increasing from 1×10^{16} As·cm^{-3} (bottom profile) to 1×10^{19} As·cm^{-3} (top profile). Inset: Variation of W_D with N_A, exhibiting an inverse relationship; $W_D \propto N_A^{-0.33}$.

Fig. 3 (a) SIMS As concentration [As] depth profile and **(b)** acceptor density and activation ratio of the absorber in the CdTe:As solar cells studied. The ~1×10^{16} As·cm^{-3} sample is unintentionally-doped and does not contain the heavily-doped (~1×10^{19} As·cm^{-3}) back-contact layer (BCL). **(c)** Typical light *J-V* curves of the CdTe:As solar cells.

Fig. 4 (a) EQE, **(b)** absorption, and **(c)** PL (glass-side) spectra of CdTe:As solar cells as function of the As concentration in the bulk. Note the step feature at 700 nm in (a) is an artefact of lamp changeover of the EQE system.

Fig. 5 PL decay curves of CdZnS/CdTe solar cells measured from the glass-side. The inset shows the extracted lifetimes, τ_1 and τ_2, obtained by fitting the decay curves with two exponentials. τ_2 is believed to represent the minority carrier lifetime in the CdTe absorber layer.

Fig. 6 V_{oc} vs. interface recombination velocity (S) between CdZnS and CdTe layers for varying acceptor concentration (N_A) and for three different conduction band offset ($\chi_{CdTe} - \chi_{CdZnS}$) values of **(a)** CBO = -0.15 eV, **(b)** CBO = 0 eV, and **(c)** CBO = +0.15 eV. A small positive CBO, i.e. spike, is beneficial for maintaining the V_{oc} when $S \geq 10^3$ - 10^4 cm·s^{-1}.

Fig. 7 V_{oc} vs. acceptor concentration (N_A) of the CdTe layer for varying donor concentrations (N_D) in the CdZnS layer, when CBO = – 0.15 eV and $S = 10^4$ cm·s^{-1}.

Fig. 8 DLTS spectra recorded for samples with various bulk As concentrations: **(a)** 1×10^{16}, **(b)** 3×10^{17}, **(c)** 4×10^{18}, and **(d)** 1×10^{19} As·cm^{-3}. Spectra were recorded over a 125 - 375K

range with a 2K increment using a pulse width of 0.1-100ms depending on the sample. Inset to (c) shows the low temperature (80 - 200K) DLTS spectrum recorded for 4×10^{18} As·cm^{-3} using a pulse width of 1 µs. Positions of observed hole (H) trap levels are labelled.

Fig. 9 Arrhenius plots of defect levels observed in DLTS spectra. Trap energy is derived from the slope with capture cross section determined from the intercept with the $\ln(\tau_e \nu_{th} N_v)$ axis.

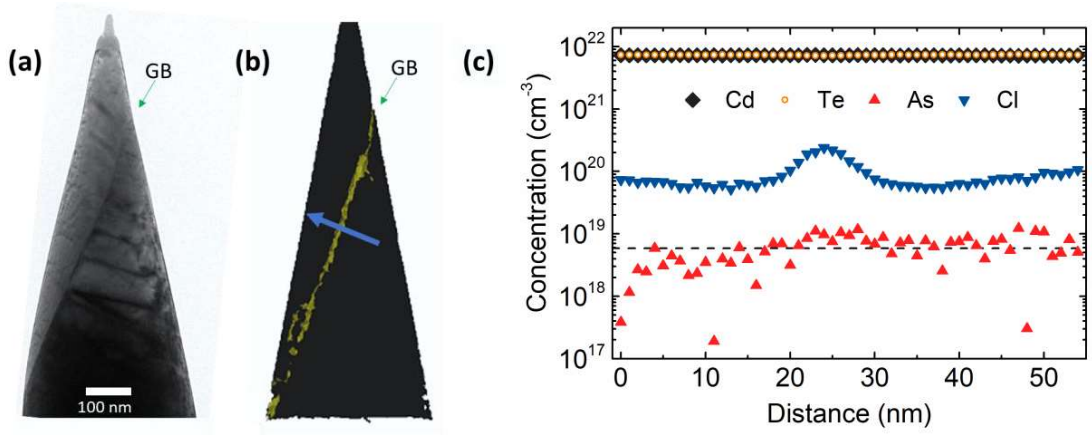

Fig. 1 A needle-shaped APT px CdTe specimen, exhibiting two grains and a GB, as imaged by TEM **(a)**. The APT reconstruction **(b)** shows a 0.9 at% Cl surface (yellow) and a 97.6 at% Cd+Te surface (black), which highlights the GB location, and the region that was used for the 1-D atomic concentration profiles of elements Cd, Te, Cl, and As **(c)** in the direction of the blue arrow in (b), derived from APT. No As accumulation, but Cl segregation can be seen around the GB. The dashed line is the mean value of As present in the region of interest.

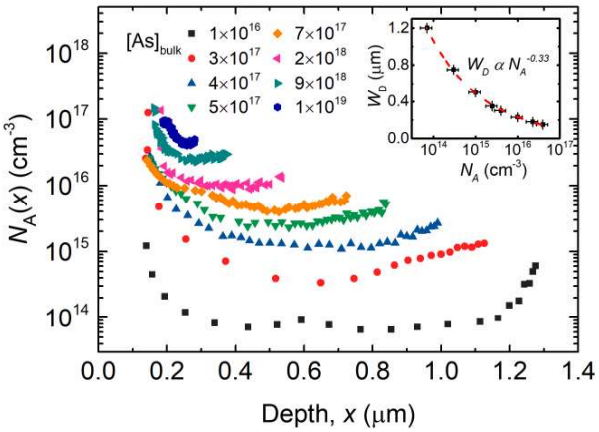

Fig. 2 Acceptor concentration (N_A) profile for px CdTe samples produced by *in-situ* doping with As concentration increasing from 1×10^{16} As·cm^{-3} (bottom profile) to 1×10^{19} As·cm^{-3} (top profile). Inset: Variation of W_D with N_A, exhibiting an inverse relationship; $W_D \propto N_A^{-0.33}$.

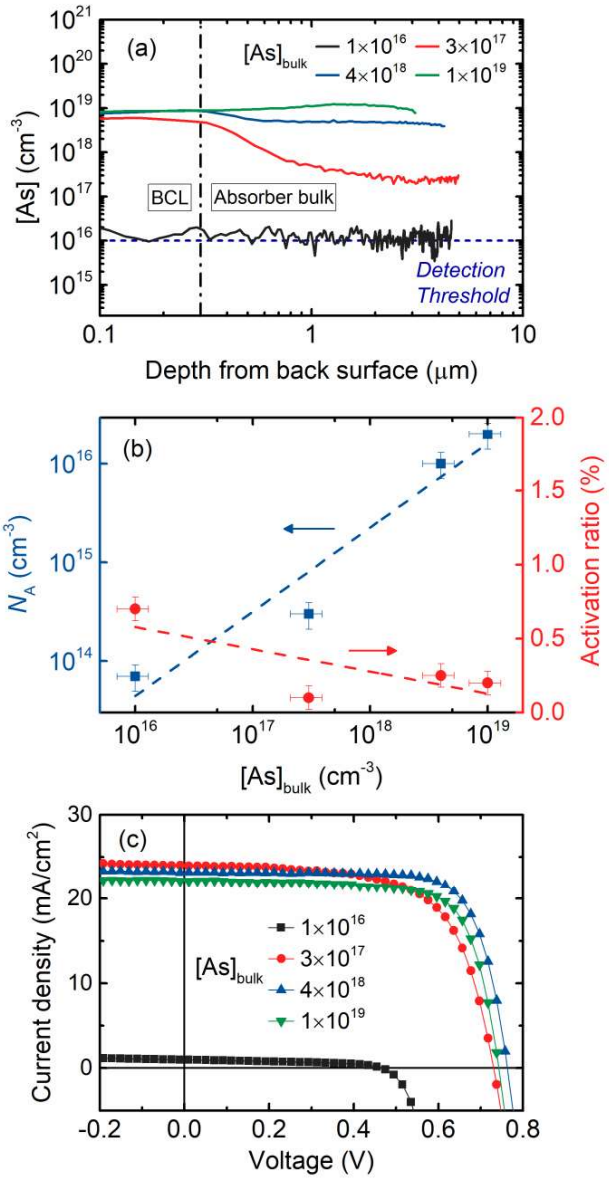
(a)
[As]bulk
1×10^16
3×10^17
4×10^18
1×10^19
[As] (cm^-3)
BCL
Absorber bulk
Detection Threshold
Depth from back surface (μm)
(b)
N_A (cm^-3)
Activation ratio (%)
[As]bulk (cm^-3)
(c)
Current density (mA/cm^2)
[As]bulk
1×10^16
3×10^17
4×10^18
1×10^19
Voltage (V)

Fig. 3 (a) SIMS As concentration [As] depth profile and **(b)** acceptor density and activation ratio of the absorber in the CdTe:As solar cells studied. The ~1×10^{16} As·cm^{-3} sample is unintentionally-doped and does not contain the heavily-doped (~1×10^{19} As·cm^{-3}) back-contact layer (BCL). **(c)** Typical light *J-V* curves of the CdTe:As solar cells.

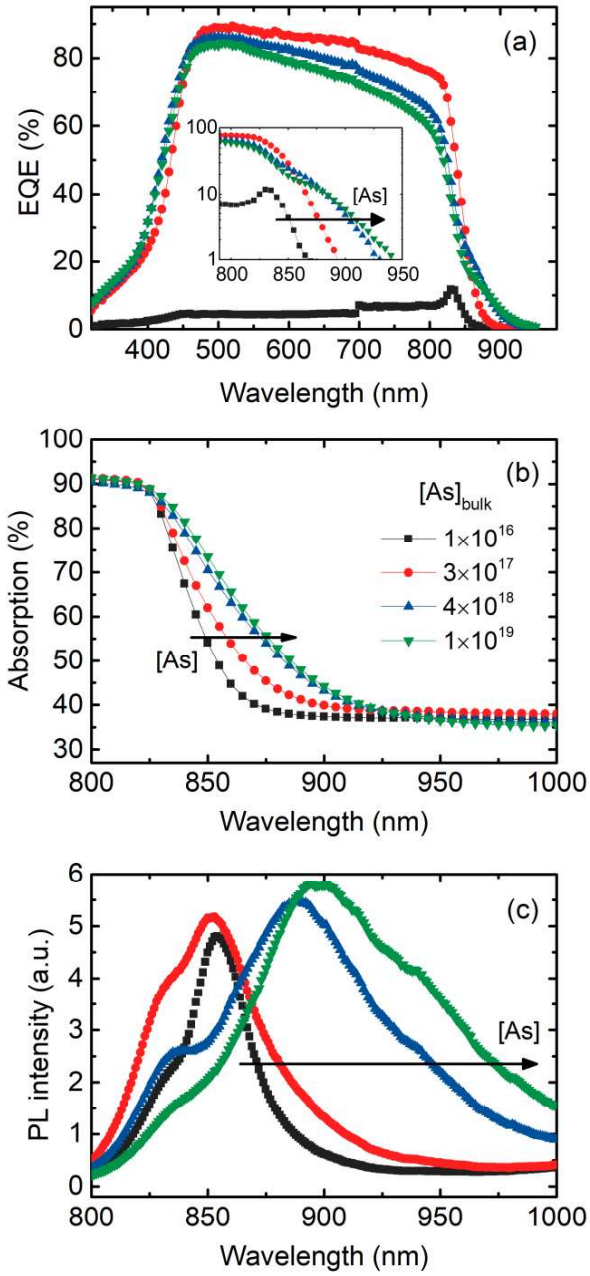

Fig. 4 (a) EQE, **(b)** absorption, and **(c)** PL (glass-side) spectra of CdTe:As solar cells as function of the As concentration in the bulk. Note the step feature at 700 nm in (a) is an artefact of lamp changeover of the EQE system.

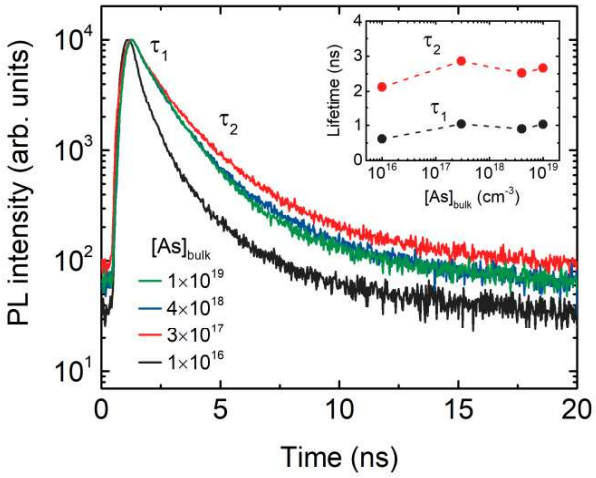

Fig. 5 PL decay curves of CdZnS/CdTe solar cells measured from the glass-side. The inset shows the extracted lifetimes, τ_1 and τ_2, obtained by fitting the decay curves with two exponentials. τ_2 is believed to represent the minority carrier lifetime in the CdTe absorber layer.

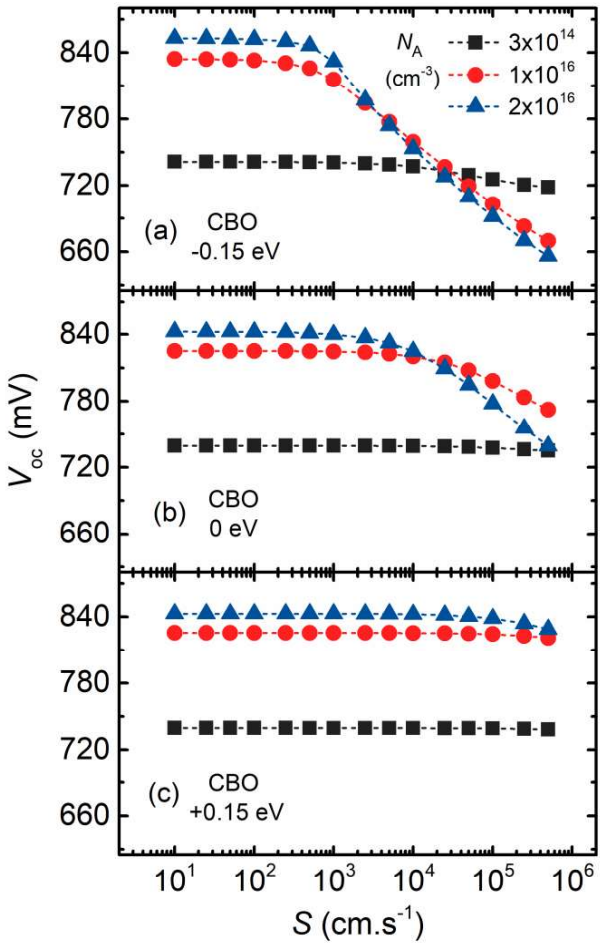

Fig. 6 V_{oc} vs. interface recombination velocity (S) between CdZnS and CdTe layers for varying acceptor concentration (N_A) and for three different conduction band offset ($\chi_{CdTe} - \chi_{CdZnS}$) values of **(a)** CBO = -0.15 eV, **(b)** CBO = 0 eV, and **(c)** CBO = +0.15 eV. A small positive CBO, i.e. spike, is beneficial for maintaining the V_{oc} when $S \geq 10^3$ - 10^4 cm·s^{-1}.

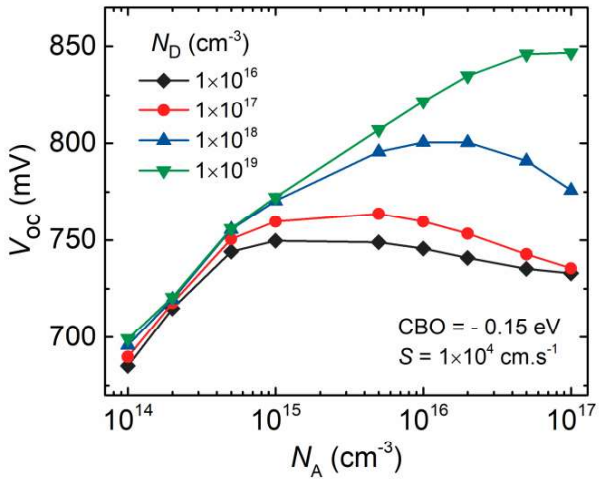

Fig. 7 V_{oc} vs. acceptor concentration (N_A) of the CdTe layer for varying donor concentrations (N_D) in the CdZnS layer, when CBO = – 0.15 eV and $S = 10^4$ cm·s^{-1}.

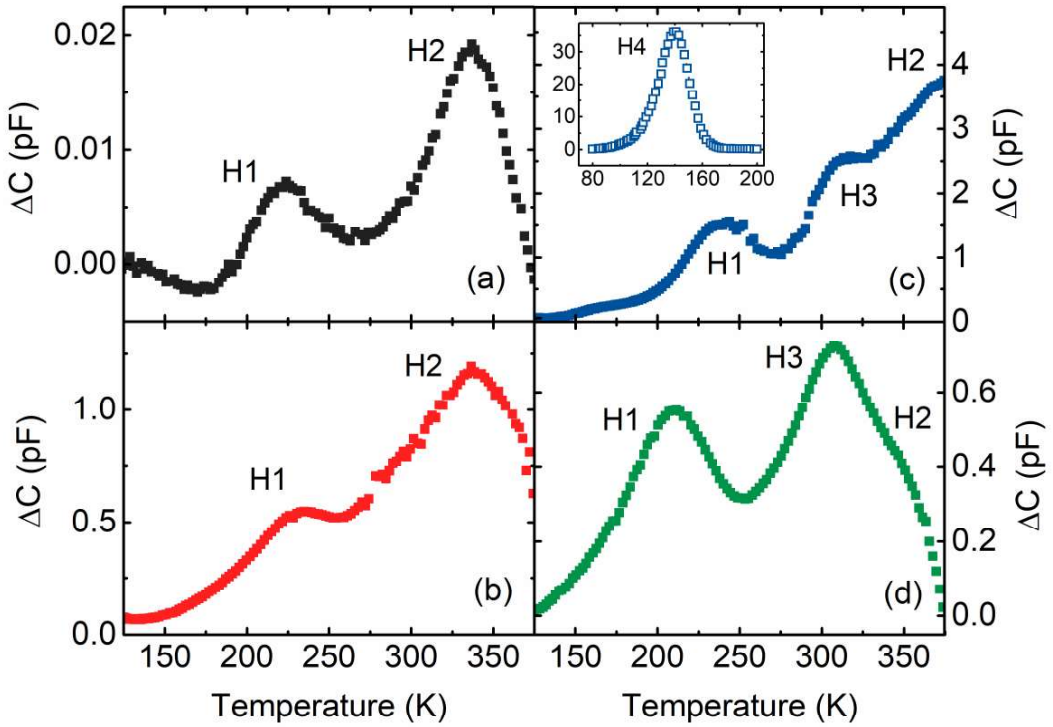

Fig. 8 DLTS spectra recorded for samples with various bulk As concentrations: **(a)** 1×10^{16}, **(b)** 3×10^{17}, **(c)** 4×10^{18}, and **(d)** 1×10^{19} As·cm^{-3}. Spectra were recorded over a 125 - 375K range with a 2K increment using a pulse width of 0.1-100ms depending on the sample. Inset to (c) shows the low temperature (80 - 200K) DLTS spectrum recorded for 4×10^{18} As·cm^{-3} using a pulse width of 1 μs. Positions of observed hole (H) trap levels are labelled.

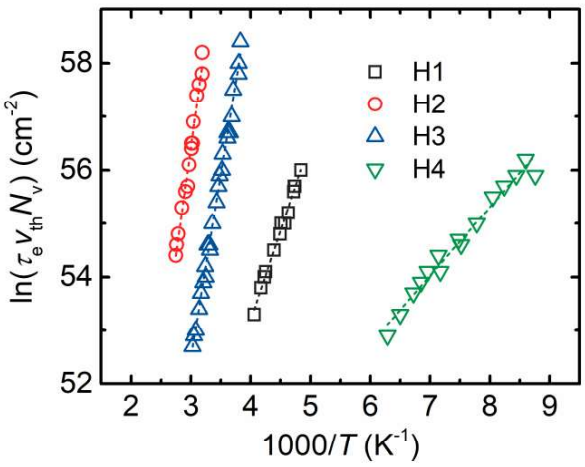

Fig. 9 Arrhenius plots of defect levels observed in DLTS spectra. Trap energy is derived from the slope with capture cross section determined from the intercept with the $\ln(\tau_e v_{th} N_v)$ axis.

Fig1a-b

Click here to download high resolution image

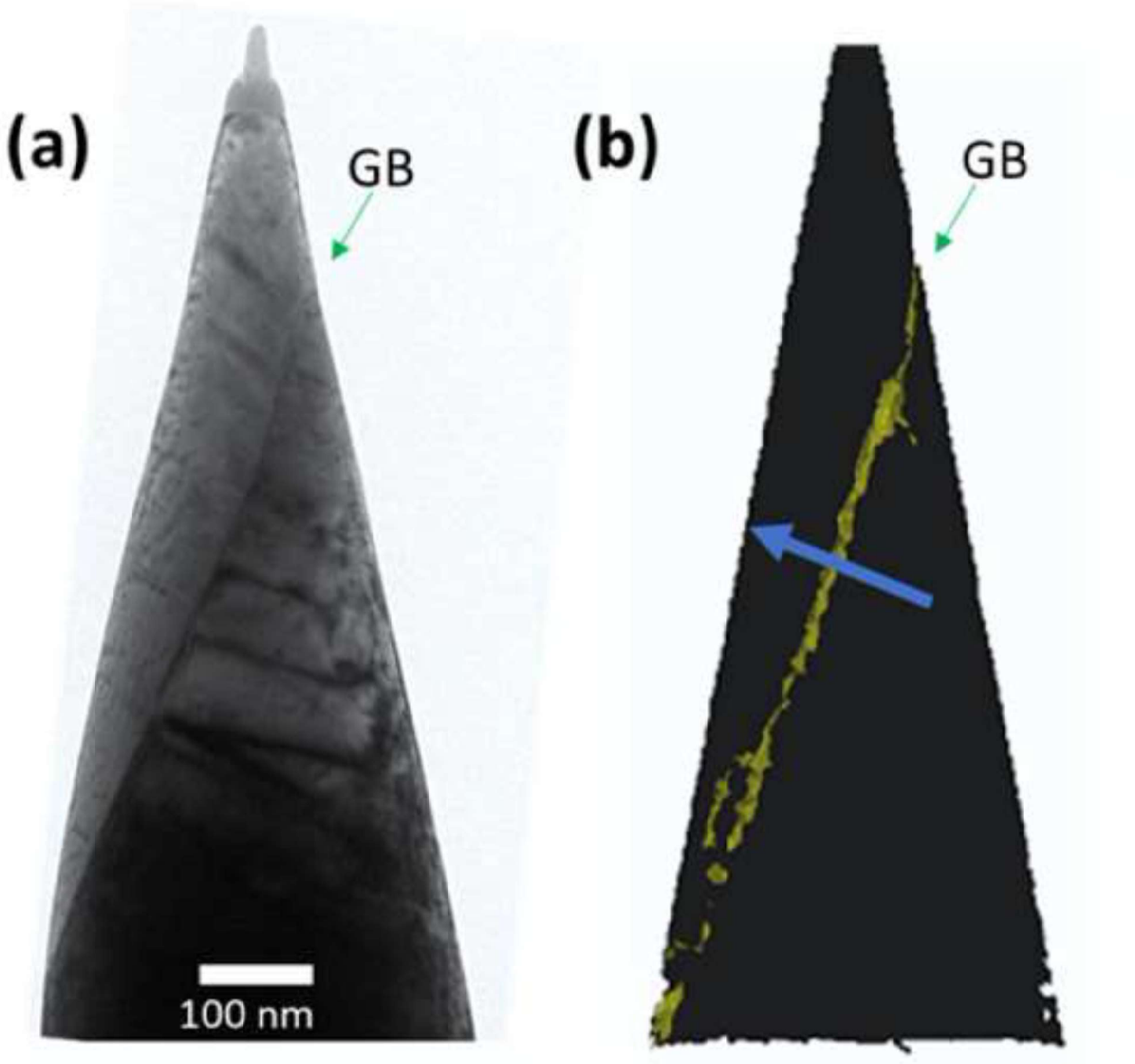

Fig1c

Click here to download high resolution image

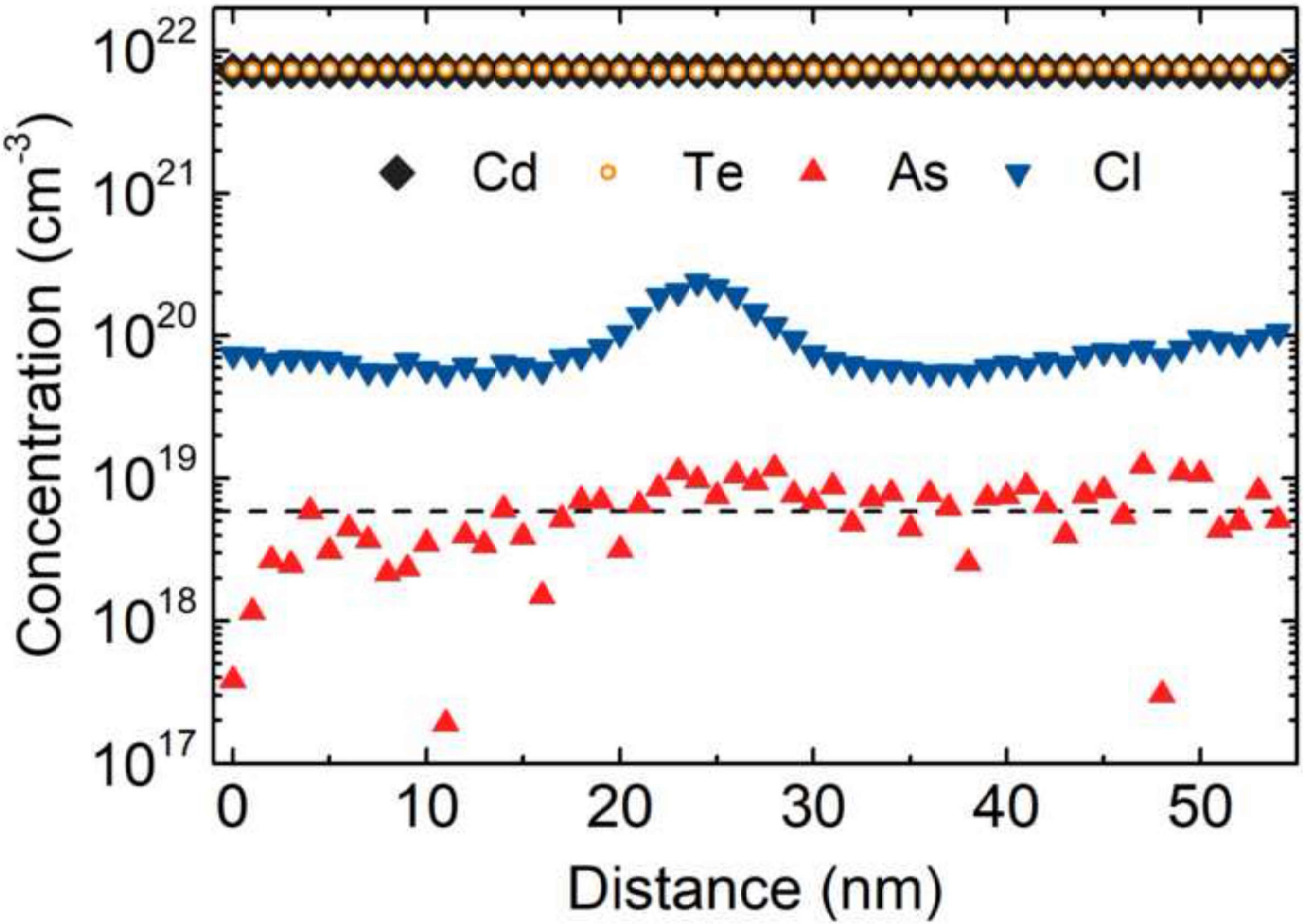

Fig2

Click here to download high resolution image

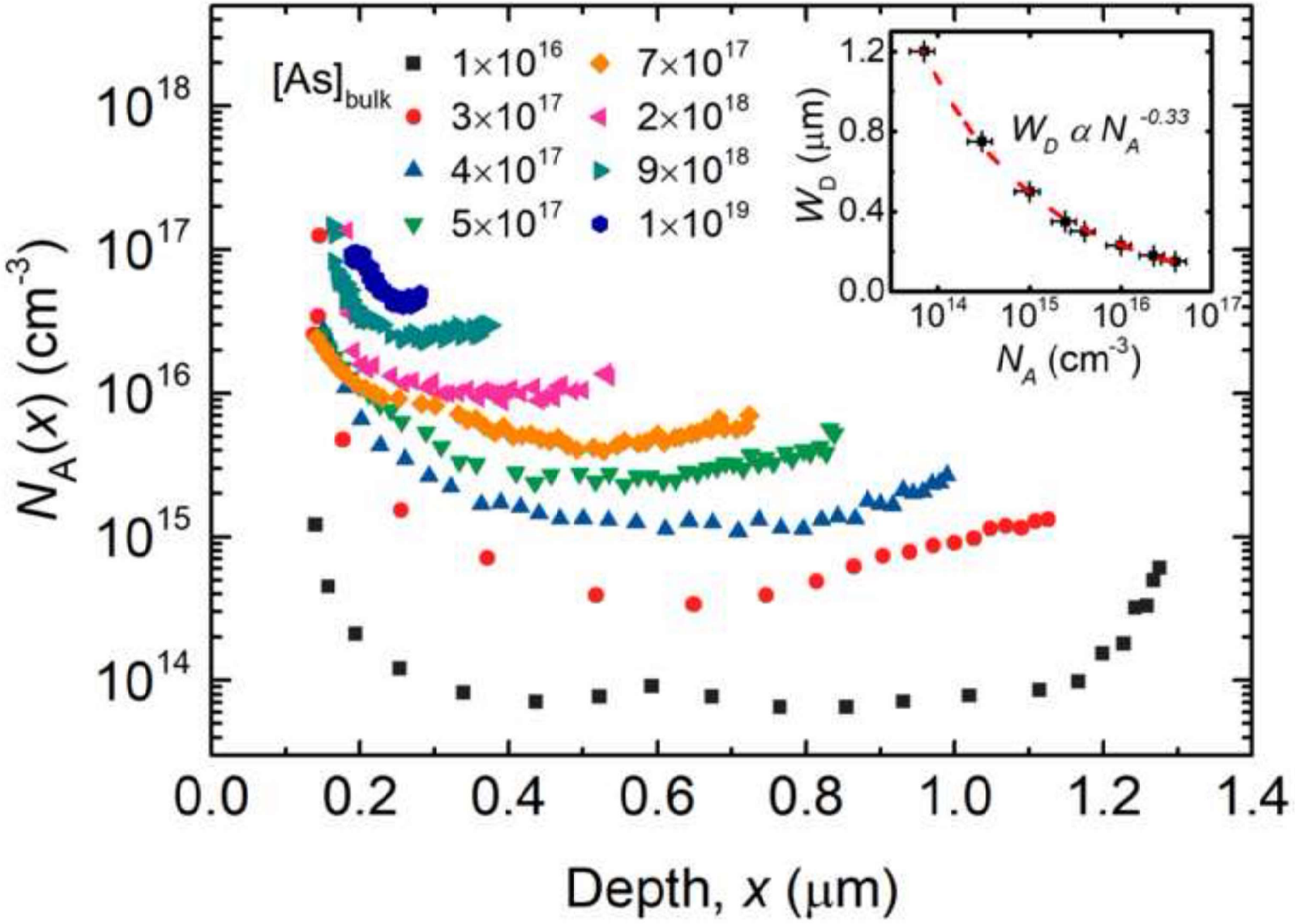

Fig3
Click here to download high resolution image

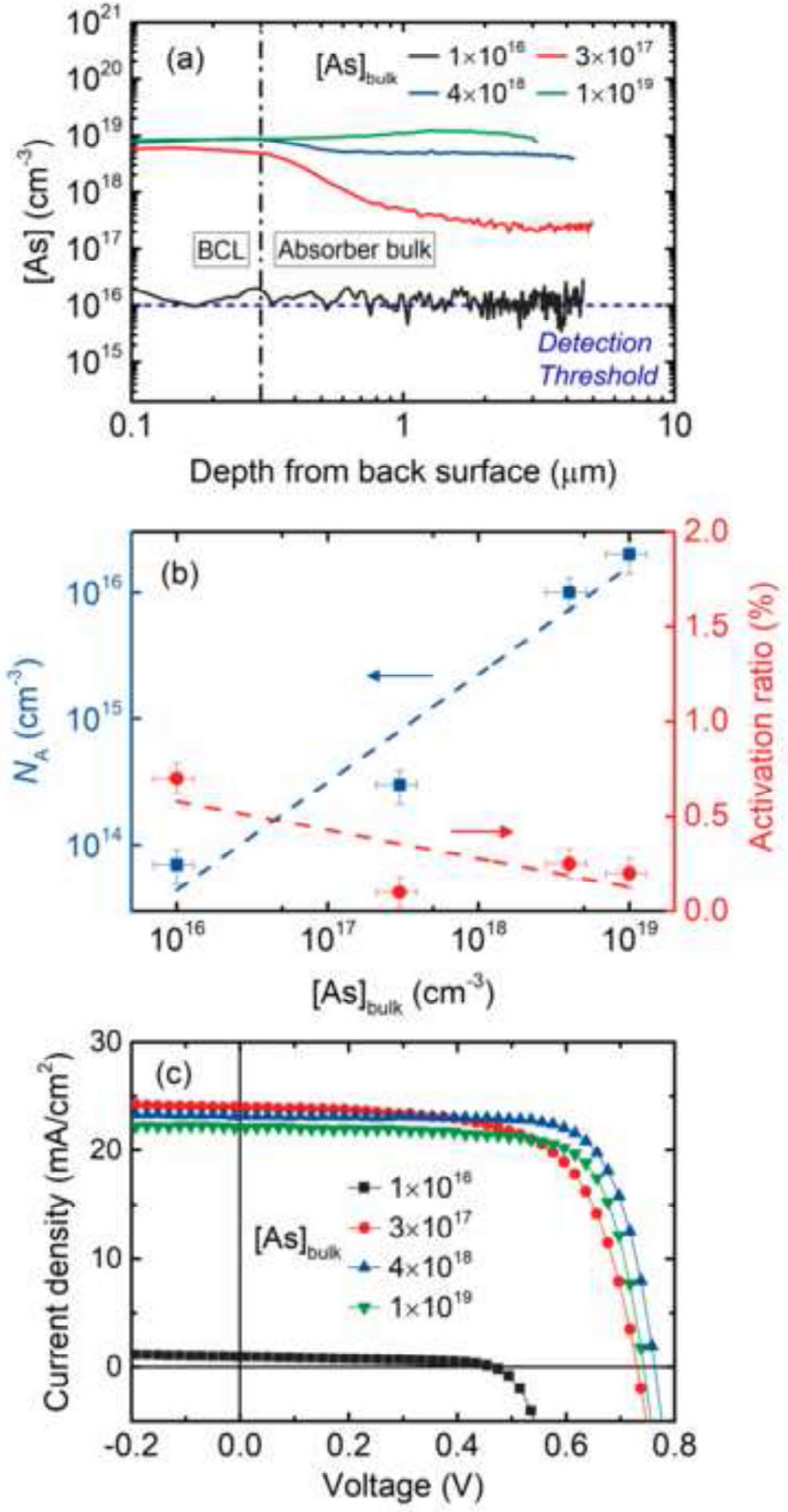

Fig4
Click here to download high resolution image

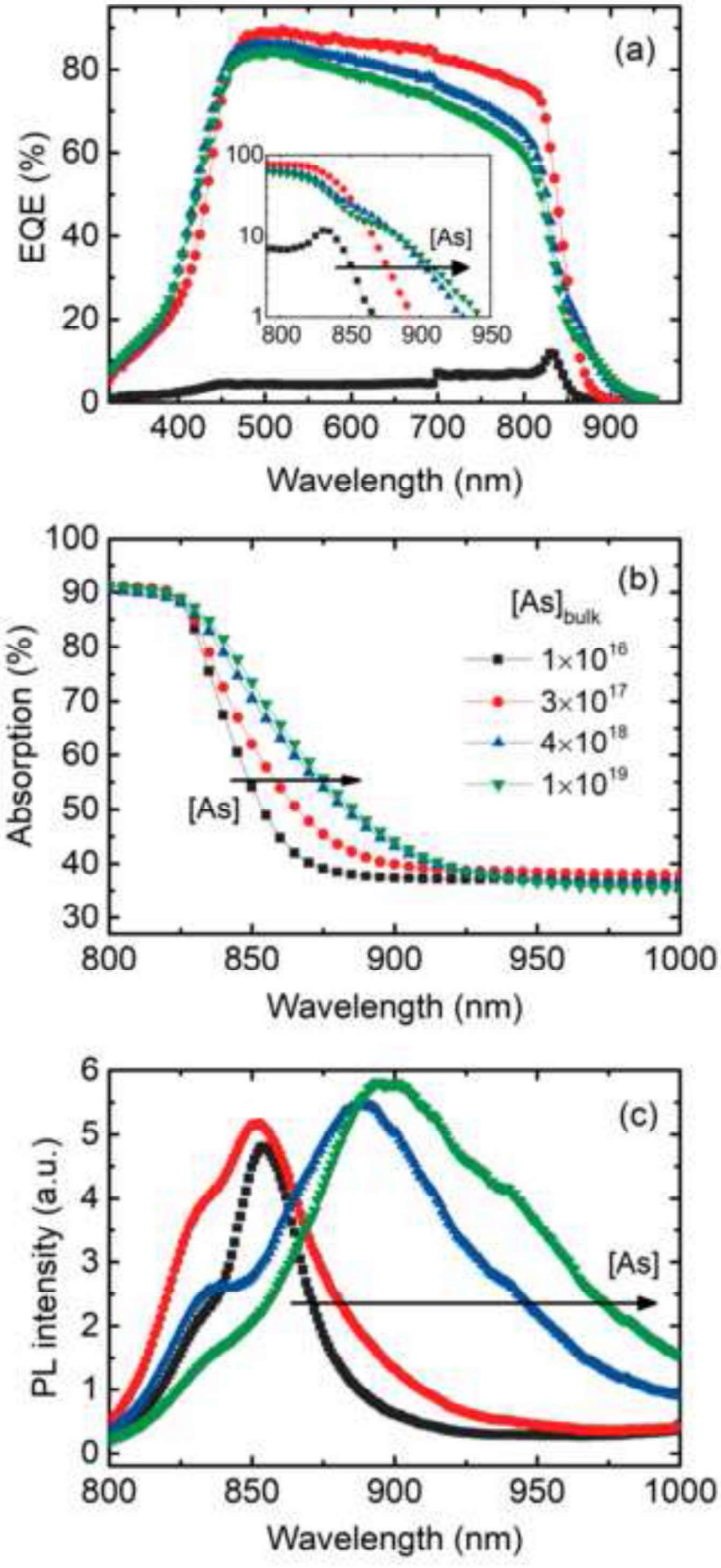

Fig5_REV

Click here to download high resolution image

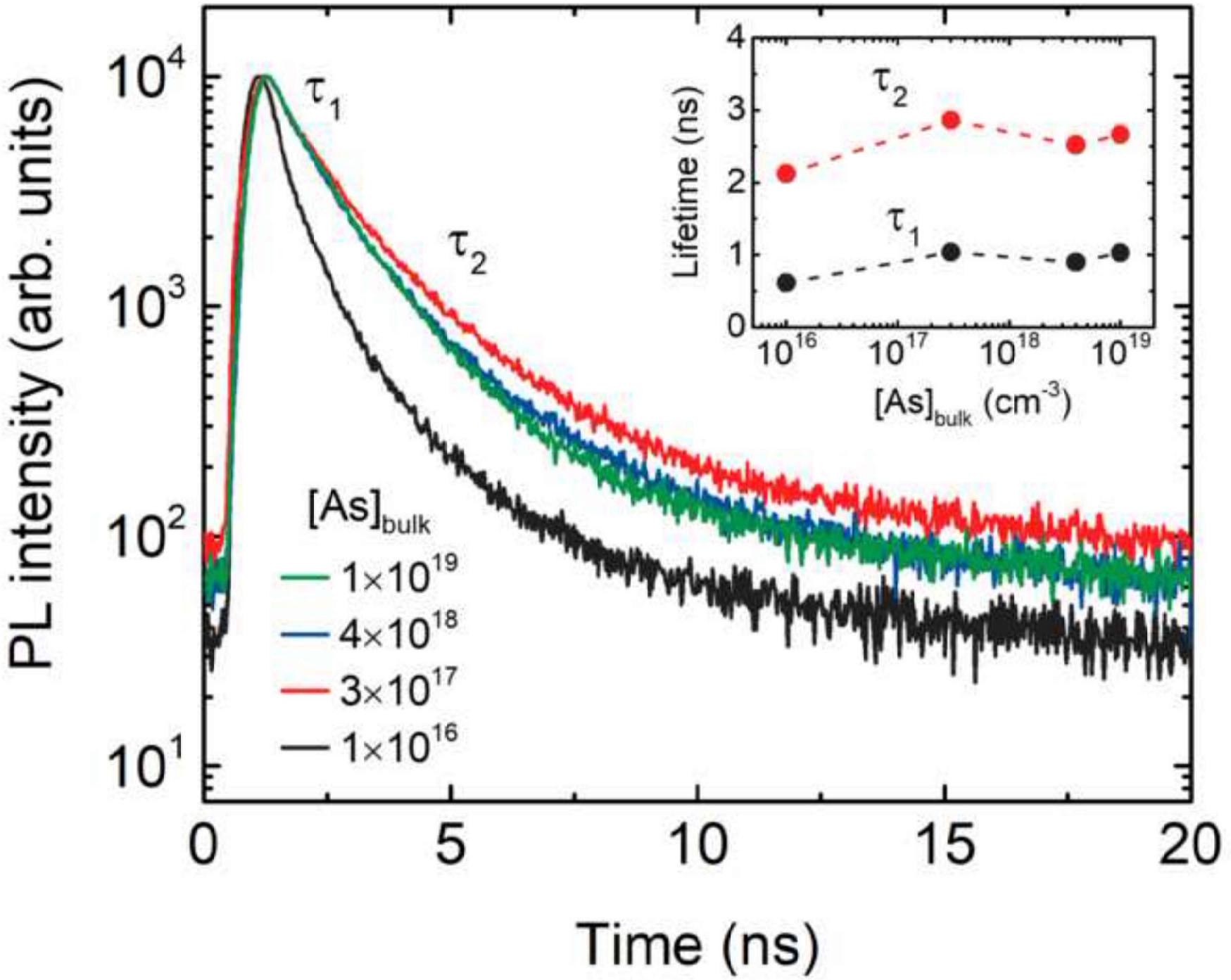

Fig6
Click here to download high resolution image

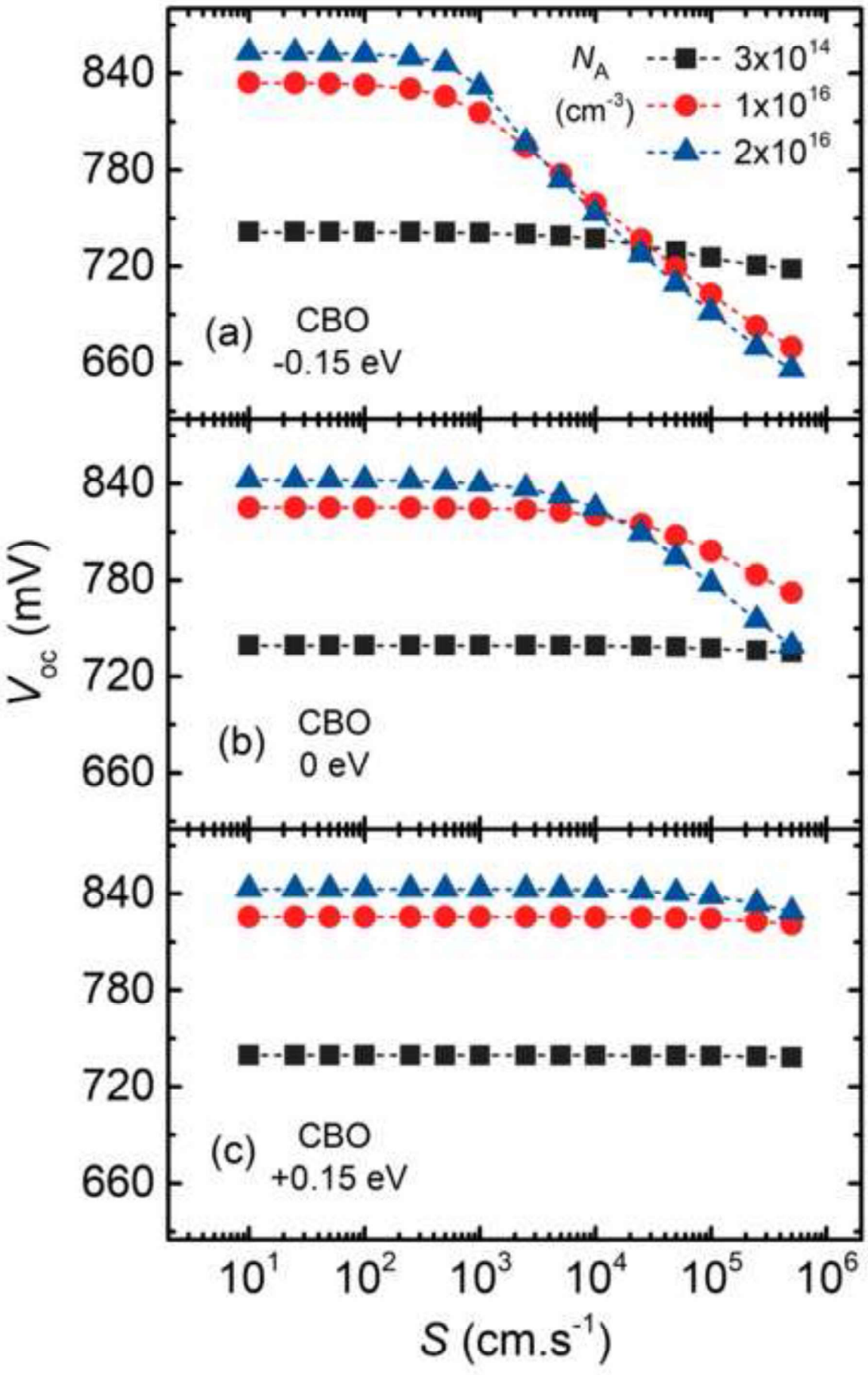

Fig7

Click here to download high resolution image

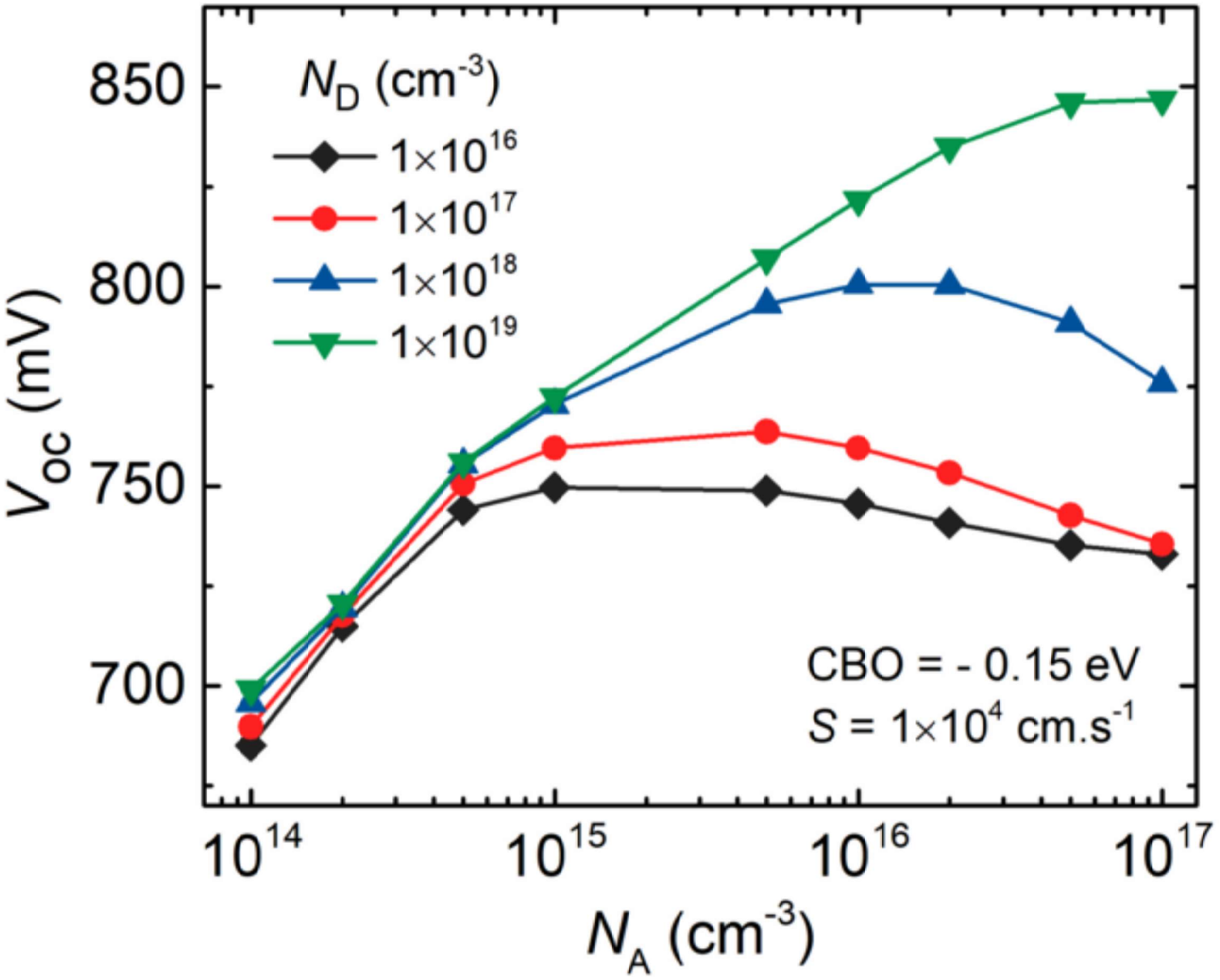

Fig8

Click here to download high resolution image

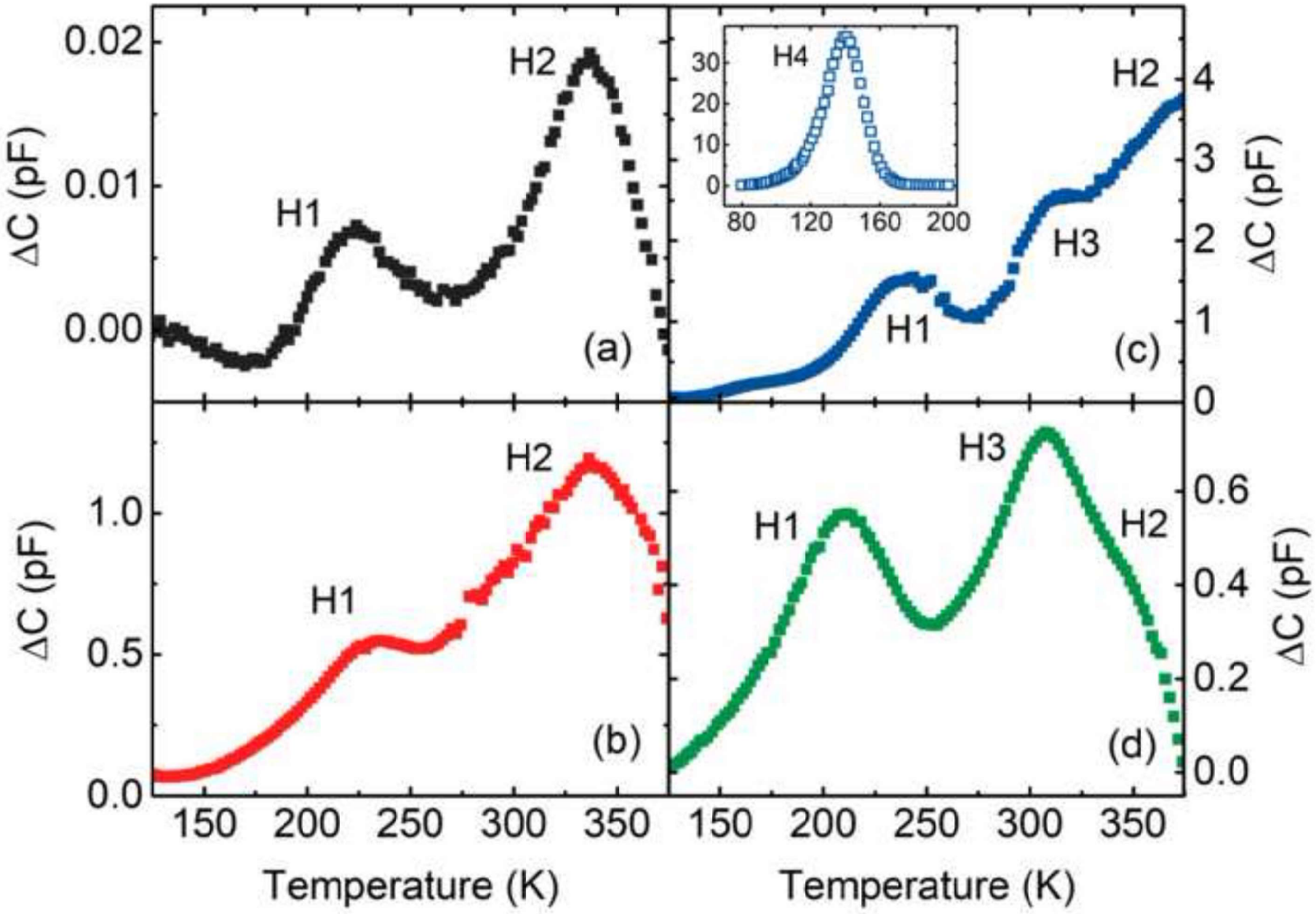

Fig9
Click here to download high resolution image

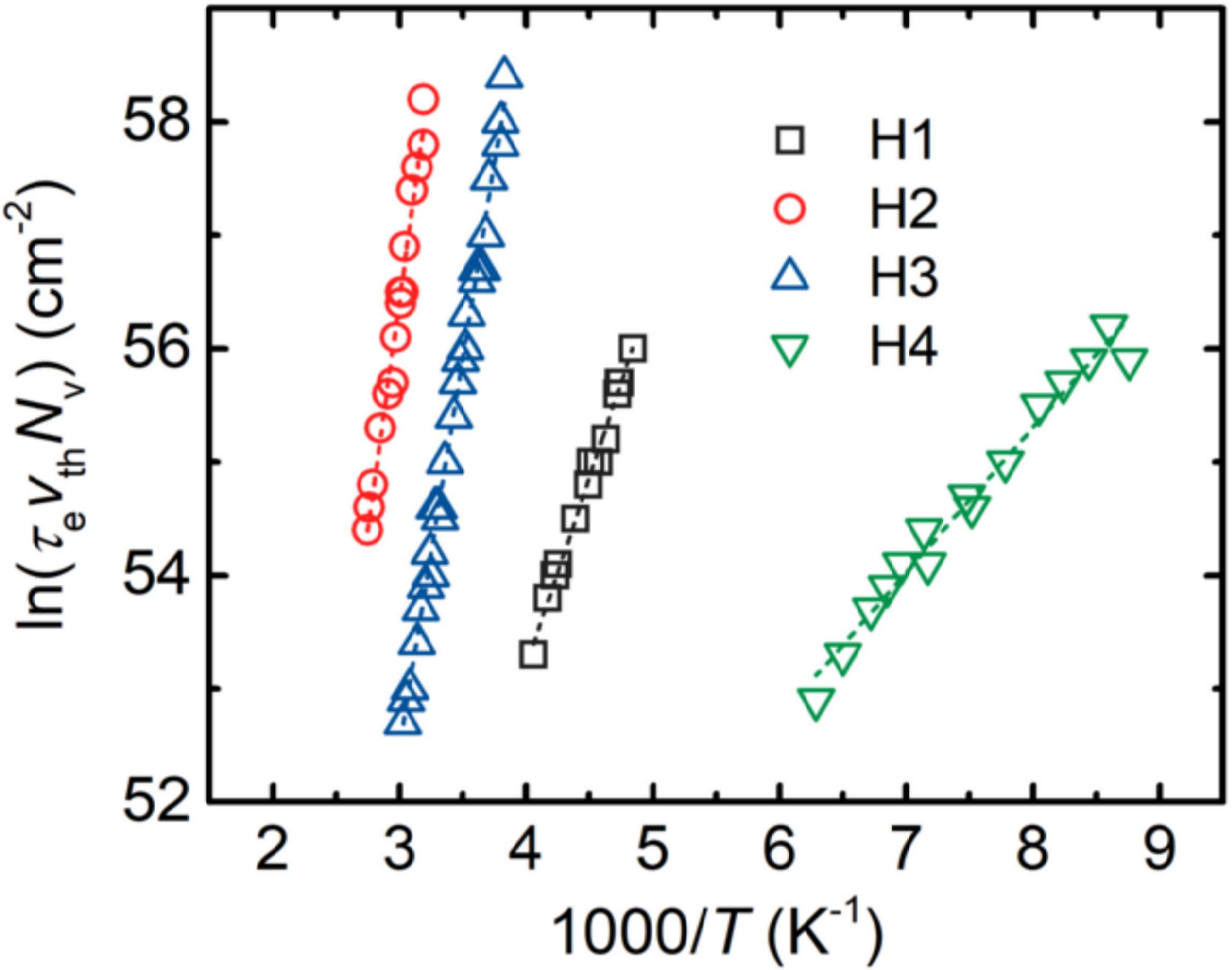

Supplementary

Click here to download Data in Brief: Supplementary_Kartopu et al.docx